Multiple phase-coherent laser pulses in optical spectroscopy. I. The technique and experimental applications

W. S. Warren and Ahmed H. Zewail

Citation: The Journal of Chemical Physics **78**, 2279 (1983); doi: 10.1063/1.445083
View online: http://dx.doi.org/10.1063/1.445083
View Table of Contents: http://scitation.aip.org/content/aip/journal/jcp/78/5?ver=pdfcov
Published by the AIP Publishing

Multiple phase-coherent laser pulses in optical spectroscopy. I. The technique and experimental applications

W. S. Warren[a] and Ahmed H. Zewail[b]

Arthur Amos Noyes Laboratory of Chemical Physics,[c] California Institute of Technology, Pasadena, California 91125

(Received 28 July 1982; accepted 4 November 1982)

In this series of papers we report on the generation and application of multiple pulse phase coherent sequences in optical spectroscopy. In this paper the effects of intense pulse trains on systems with only two resonant energy levels are analyzed, with particular attention to the effects of extreme inhomogeneous broadening and population depletion to nonresonant levels. It is shown that these effects, which are present in virtually all optical systems, make the simple gyroscopic model of optical coherent transients invalid. Exact calculations show, e.g., that a two-pulse photon echo is not maximized by a 1:2 length ratio for the pulses; that the maximum excited state population is not created by a 180° pulse; and that three equal pulses are almost as effective as a 1:2:1 ratio for producing three pulse echoes. The role of pulse phase is extensively analyzed. Pulse sequences are proposed and experimentally demonstrated which permit optical phase sensitive detection and measurement of ground state relaxation parameters. The experimental results are based on an extension of the acousto-optic modulation and fluoresence detection techniques of Zewail and Orlowski [Zewail *et al.*, Chem. Phys. Lett. **48**, 256 (1977); Orlowski *et al.*, *ibid.* **54**, 197 (1978)]. The relative merits of fluorescence and transverse polarization detection are discussed, and fluorescence detection is shown to be more generally useful for these new sequences. Finally, composite pulse trains are shown to be capable of substantially increasing the signal available from highly inhomogenously broadened transitions. In paper II we extend the treatment to multilevel systems with some emphasis on solid state applications.

I. INTRODUCTION

It has been amply demonstrated over the last 30 years that a molecule which is exposed to a coherent radio frequency or microwave pulse can absorb energy and then coherently reradiate it.[1–18] Pulsed nuclear magnetic resonance (NMR) in particular has evolved into an extremely powerful spectroscopic tool, largely because one can generate highly complex yet stable pulse trains with independently adjustable pulse delays, intensities, durations, and phases. As a result, within broad limits any pulse sequence which can be written down can be executed, and many different sequences have been reported.

This phase-coherent multiple pulse capability is of great value to multilevel systems, but would be of little use if all samples could be treated as if they contained only noninteracting spins; an ensemble of noninteracting spins $\frac{1}{2}$, e.g., can be treated statistically as a two-level system, and such a small system can be completely characterized by measuring only a few parameters. But most modern NMR experiments are concerned with much larger systems. A set of N coupled protons has 2^N energy levels and $2^N(2^N-1)$ possibly nondegenerate transitions. Measurement of the couplings gives useful information on intermolecular and intramolecular interactions. However, the resulting spectra are complicated. The main role of multiple phase trains has been to simplify these spectra. For example, pulse trains have been designed to eliminate inhomogeneous broadening or chemical shifts in highly coupled systems,[8,9] eliminate the direct dipole–dipole or quadrupole interaction to measure chemical shift tensors orders of magnitude smaller[10–12]; pump forbidden transitions,[13–15] sometimes with high intensity[16]; avoid pumping some allowed transitions to overcome dynamic range problems in dilute samples[17]; and resolve different spin interactions through two-dimensional Fourier transformation.[18] In fact, the majority of current NMR research would probably be impossible without the capability to apply more than one pulse and to know the precise phase relation between these pulses.

The first optical coherent experiments were direct analogs of NMR sequences to study two-level systems, sometimes with different results reflecting the effects of pulse propagation and coupling to Maxwell's equations. The r-vector model of optical coherence[19,20] helps to give physical insight in these cases. However, true optical two-level systems are quite rare. As we shall show, under real experimental conditions transition inhomogeneities, high densities of states, and relaxation to other states make such a simplification in many cases invalid.

The optical analog of NMR multiple pulse generation is difficult to achieve simply because the wavelength of the light is much shorter than the rf wavelength, and phase randomization on this "distance scale" is quite large. In a recent communication,[21] we have shown that the techniques of acousto-optic modulation and fluorescence detection, which were introduced by Zewail and Orlowski[22] to observe photon echoes on the spontaneous emission of molecules, can be extended to circumvent this problem, thus leading to the development of phase-coherent multiple pulse spectroscopy in the optical domain.

---

[a] National Science Foundation Postdoctoral Fellow, 1981. Present address: Department of Chemistry, Princeton University, Princeton, New Jersey 08544.

[b] Alfred P. Sloan Foundation Fellow and Camille and Henry Dreyfus Foundation Teacher-Scholar.

[c] Contribution No. 6647.

 0021-9606/83/052279-19$2.10

In this and the following paper we give a full account of the technique and its application to optical multilevel systems. Specifically, in this paper we shall calculate the effects of several simple pulse sequences on optical systems with only two nearly resonant energy levels, although many other levels may be indirectly involved. In a few cases the results are consistent with what might be predicted from a simple two-level approximation; more often, however, the intuition gained from such an approximation is inaccurate, and an explicit multilevel treatment gives a much better understanding of intermolecular interactions, inhomogeneous vs homogeneous broadening, and relaxation mechanisms. We also present the experimental principles behind the generation of phase coherent pulses by acousto-optic modulation[22] and apply the technique to molecular gases. In paper II we report on the extension to multilevel systems as solids, and in a third paper we treat selective multiquantum excitation.

II. THEORY OF MULTIPLE PULSE TRAINS

A. Hamiltonian for two-level systems: NMR and optical

The theoretical framework for understanding closed two-level systems has been detailed in many articles and textbooks[4,5,20] and we will only summarize it here to establish our notation. The Hamiltonian which describes the interaction of a static field B_0 along the laboratory $\hat{z}$ axis and a radio-frequency field $B_1(t)$ along the laboratory x axis with an ensemble of noninteracting spins $-\frac{1}{2}$ is

$$\mathcal{H} = -\boldsymbol{\mu}\cdot\mathbf{B} \equiv -\hbar\omega_1(t)\cos[\omega t+\phi(t)]I_x - \hbar\omega_0 I_z\,, \tag{1}$$

$$\omega_0 = \gamma B_0\,, \tag{2}$$

$$\mathbf{B}_1(t) = \gamma^{-1}\omega_1(t)\cos[\omega t+\phi(t)]\hat{x}\,, \tag{3}$$

where γ is the gyromagnetic ratio. The concept of phase is intuitively obvious at radio frequencies, perhaps because the experimentalist can actually see the sinusoidal oscillations of a rf pulse on an oscilloscope. If both $\omega_1(t)$ and $\phi(t)$ change only slightly in any interval of length $1/\omega$ (the "slowly varying envelope approximation"[23]) then the pulse sequence can be viewed as having a carrier frequency ω, with some amplitude modulation $\omega_1(t)$ and phase $\phi(t)$. If it is further assumed that terms in the Hamiltonian corresponding to high frequencies can be neglected (the "rotating wave approximation"[24]) the Hamiltonian becomes

$$\mathcal{H} = -\hbar\,\Delta\omega I_z - \hbar\omega_1(t)\cos\phi(t)I_x - \hbar\omega_1(t)\sin\phi(t)I_y\,, \tag{4}$$

$$\Delta\omega = \omega-\omega_0 = \overline{\Delta\omega}+\Delta\omega(q)\,. \tag{5}$$

The resonance offset $\Delta\omega$ is frequently not identical for all members of the ensemble. To reflect this we have decomposed $\Delta\omega$ into an average offset $\overline{\Delta\omega}$ and a term $\Delta\omega(q)$ which depends on some generalized sample coordinate q (usually position).

The electric field amplitude at laser frequencies must usually be described by a more complicated expression than Eq. (1) because the wavelength is usually much smaller than the spatial volume of interest. Still neglecting inhomogeneities we can generally write, for traveling plane waves

$$\mathbf{E}(r,t) = [\hat{\epsilon}(t)]\mathcal{E}(t)\exp\{i[\mathbf{k}(t)\cdot\mathbf{r}-\omega t+\Phi(t)]\}, \tag{6}$$

where $\mathbf{k}$ is the wave vector and $\hat{\epsilon}$ is the polarization direction. We will define the phase $\phi(r,t)=\mathbf{k}\cdot\mathbf{r}+\Phi(t)$. The concept of the phase of a time varying electric field clearly corresponds to a semiclassical picture. In a fully quantized picture each distinct state of the quantized radiation field has photon number and phase operators which do not commute,[25] so the phase and amplitude cannot be independently fixed. However, a coherent state of the quantized field with a large number of photons will simultaneously have only a small fractional uncertainty in the amplitude and the phase, approximating the semiclassical limit.[25] Thus the concept of pulse phase is still well defined. If $\mathcal{E}(t)$ and $\Phi(t)$ are assumed to vary little in any time interval of length ω^{-1}, then $\mathcal{E}(t)$ can be viewed as an amplitude modulation and $\Phi(t)$ as a phase modulation on some carrier wave at frequency ω.

The semiclassical interaction between an electric field and matter has the form $\boldsymbol{\mu}\cdot\boldsymbol{\mathcal{E}}$, where $\boldsymbol{\mu}$ is the transition dipole moment. This clearly has the same form as the rf interaction with a spin in Eq. (1) except that the $\mathbf{k}\cdot\mathbf{r}$ term introduces propagation effects. In the NMR case the static field establishes an energy difference between the ground and excited states. In the optical case, this energy difference is established by other terms in the total electronic Hamiltonian. In either case the energy difference appears in a two-level Hamiltonian as

$$\mathcal{H}_{\rm diag} = \begin{pmatrix} \frac{1}{2}\hbar\omega_0 & 0 \\ 0 & -\frac{1}{2}\hbar\omega_0 \end{pmatrix}\,, \tag{7}$$

with

$$\omega_0 = (E_{\rm excited}-E_{\rm ground})/\hbar\,. \tag{8}$$

Defining R_1, R_2, and R_3 as[19,20]

$$R_1 = \begin{pmatrix} 0 & \frac{1}{2} \\ \frac{1}{2} & 0 \end{pmatrix},\quad R_2 = \begin{pmatrix} 0 & -i/2 \\ i/2 & 0 \end{pmatrix},\quad R_3 = \begin{pmatrix} \frac{1}{2} & 0 \\ 0 & -\frac{1}{2} \end{pmatrix} \tag{9}$$

allows the optical rotating frame Hamiltonian to be written as

$$\mathcal{H}(r,t) = -\hbar\Delta\omega R_3 - \hbar\omega_1(t)\cos[\phi(r,t)]R_1 - \hbar\omega_1(t)\sin[\phi(r,t)]R_2\,, \tag{10}$$

$$\phi(r,t) = \Phi(t)+\mathbf{k}\cdot\mathbf{r}\,, \tag{11}$$

which is directly analogous to the NMR case [Eq. (4)] with the assignments $I_x \longrightarrow R_1$, $I_y \longrightarrow R_2$, $I_z \longrightarrow R_3$. The R_3 term is sometimes attributed to the interaction of a fictitious $\hat{z}$-axis polarization with a fictitious static electric field,[20] to make the NMR and optical Hamiltonians "physically" identical. For the rest of this paper we will use Pauli matrices σ_x, σ_y, and σ_z when either R or I would be correct.

B. Density matrix evolution and relaxation

In the absence of relaxation, the density matrix (for fixed $\mathbf{r}$ and $\mathbf{q}$) evolves as

$$\dot{\rho}(t) = +i\hbar^{-1}[\rho(t),\mathcal{H}(t)]\,, \tag{12}$$

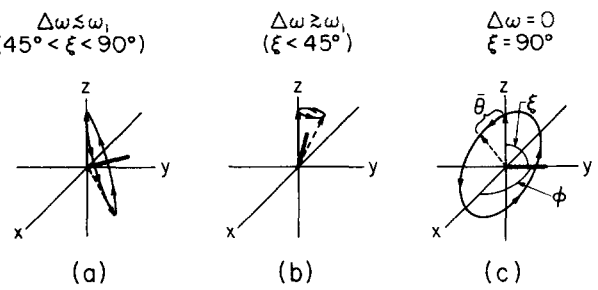

FIG. 1. The rotations of magnetization or pseudopolarization generated by pulses with different ratios of resonance offset $\Delta\omega$ to pulse bandwidth ω_1. When $\Delta\omega \neq 0$ [part (a)] an initial z-axis component is rotated along a cone of full width 2ξ, where $\xi = \tan^{-1}(\omega_1/\Delta\omega)$, and the initial position (proportional to the population difference between the ground and excited states) cannot be completely inverted. The cone narrows as $\Delta\omega$ increases, as shown in part (b). When $\Delta\omega = 0$ complete population inversion is possible, as shown in part (c).

which can be integrated over intervals such that $\mathcal{H}(t) \equiv \mathcal{H}$ is time independent:

$$\rho(t) = \exp(-i\mathcal{H}t/\hbar)\rho(0)\exp(i\mathcal{H}t/\hbar) \ . \tag{13}$$

In NMR one usually uses pulses with approximately square envelopes, so during any particular pulse the rotating frame Hamiltonian [Eq. (4)] is indeed time independent. Equation (13) implies that the Hamiltonian generates a simple rotation about an axis determined by $\Delta\omega$ and ϕ. More precisely, the propagator for a single pulse with intensity ω_1, length t, flip angle $\theta = \omega_1 t$, phase ϕ, and resonance offset $\Delta\omega$ is

$$U = \exp\{-i[\Delta\omega\sigma_z + (\omega_1\cos\varphi)\sigma_x + (\omega_1\sin\varphi)\sigma_y]t\}$$

$$= \begin{pmatrix} \cos\frac{1}{2}\bar{\theta} - i\sin\frac{1}{2}\bar{\theta}\cos\xi & -ie^{-i\varphi}\sin\frac{1}{2}\bar{\theta}\sin\xi \\ -ie^{+i\varphi}\sin\frac{1}{2}\bar{\theta}\sin\xi & \cos\frac{1}{2}\bar{\theta} + i\sin\frac{1}{2}\bar{\theta}\cos\xi \end{pmatrix} , \tag{14}$$

$$\bar{\theta} = \sqrt{(\Delta\omega)^2 + \omega_1^2}\,t = \theta\sqrt{1 + (\Delta\omega/\omega_1)^2} \ , \tag{15}$$

$$\xi = \tan^{-1}\left(\frac{\omega_1}{\Delta\omega}\right) \text{ if } \Delta\omega > 0 \ ;$$
$$\xi = \pi + \tan^{-1}\left(\frac{\omega_1}{\Delta\omega}\right) \text{ if } \Delta\omega < 0 \ . \tag{16}$$

Such a pulse generates a rotation of $\bar{\theta}$ radians about an axis with spherical coordinates $(\phi, (\pi/2) - \xi)$ [Figs. 1(a) and 1(b)]. If the initial magnetization or polarization is proportional to σ_z, then it is constrained to stay along a fixed cone (determined by the initial position and the rotation axis) no matter how large $\bar{\theta}$ is. The largest change is produced by a pulse with $\bar{\theta} = (2n+1)\pi$; a pulse with $\bar{\theta} = 2n\pi$ has no effect. If $\Delta\omega = 0$ [Fig. 1(c)] all rotations are about an axis in the xy plane and this is the case most commonly encountered in NMR.

Under the following simplifying conditions the mathematics is similar for optical spectroscopy:

(1) All pulses are assumed to have the same polarization direction.

(2) Propagation effects (e.g., nonlinear coupling to Maxwell's equations and attenuation of the beam by the sample) are ignored.

Condition (1) makes the definition of a "pseudopolarization" vector identical for each pulse. Condition (2) excludes self-induced transparency, optical density effects, and similar effects.[25]

If all pulses are collinear the situation simplifies further, since the relative phase between two pulses is then not a function of position. Finally, if $\mathcal{E}(t)$ corresponds to essentially square pulses and $\phi(t)$ is constant during any individual pulse, then the role of the phase is identical in the optical and NMR cases. Calculating the effects of more general pulses, such as a Gaussian pulse intensity profile, requires a more complicated treatment since the rotation axis ξ is time dependent. In such cases there still exists a unitary transformation U such that

$$\rho(t) = U\rho(0)U^* \ . \tag{17}$$

U is most conveniently found by decomposing the actual intensity profile into a set of step functions covering intervals which are short compared to the rate of change of the envelope, calculating the propagators for these small pieces, and multiplying them together.

The net effect of more than one pulse is, of course, a product of rotations. Therefore, starting from the equilibrium density matrix, Eqs. (13) and (14) can be used to calculate the exact final density matrix for any sequence. In either the NMR or optical case a Boltzmann equilibrium distribution is achieved:

$$\rho_{eq} = \exp(-\mathcal{H}/kT)/\mathrm{Tr}[\exp(-\mathcal{H}/kT)] \ , \tag{18}$$

where T is the temperature and k the Boltzmann constant. The energy difference between the two states is much less than kT in almost all NMR experiments, and much larger than kT for most optical experiments. Equation (18) then can be rewritten as

$$\rho_{eq} = 1 - \beta\sigma_z \ , \tag{19}$$

where $\beta = 1$ in the optical case, $\beta \ll 1$ in NMR, and 1 is the identity matrix divided by two.

The situation becomes more complicated when relaxation effects are included, since even a time independent Hamiltonian does not then generate a unitary transformation. One can often write the density matrix evolution as ($\hbar = 1$)

$$\dot{\rho}(t) = +i[\rho(t), \mathcal{H}(t)] + R \ ,$$

$$R = \begin{pmatrix} -(\rho_{11} - \rho_{11}^0)/T_1 & -\rho_{12}/T_2 \\ -\rho_{21}/T_2 & -(\rho_{22} - \rho_{22}^0)/T_1 \end{pmatrix} , \tag{20}$$

where ρ_{11}^0 and ρ_{22}^0 are the equilibrium populations of the two states (this is the density matrix form of the Bloch[1] equations). If relaxation during the pulses can be neglected, the effect of R during pulse sequence delays is to cause the off-diagonal elements to damp out with time constant T_2, and the equilibrium population distribution to be restored at a rate T_1. A more versatile approach, but one which requires manipulations of larger matrices, is to switch to a superoperator representation.[26–28]

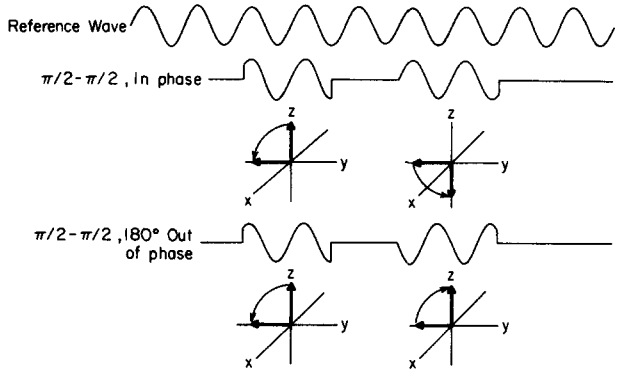

FIG. 2. A simple illustration of the effects of the relative phase of two pulses. The 90° pulses on resonance create a complete population inversion if they are in phase with one another; they have no net effect if they are exactly out of phase. Thus, if the relative phase is not specified little is known about the final state of the system. The role of pulse phases is discussed in greater detail in the text.

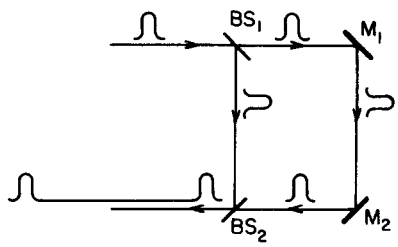

FIG. 4. Generation of laser multiple pulse trains by splitting a single pulse. The delay between the two output pulses is the time needed for light to travel the path length difference. The relative phase is determined by the exact number of wavelengths in this path difference, and changes by 2π whenever the difference changes by λ. A 10 ns (10 f) delay must then be stable, measurable, and settable to 1 part in 10^7 to know the relative phase. As a result, this approach is generally used only if phase is unimportant, as occurs for two-pulse photon echoes but not for more complex sequences.

III. GENERATION OF PHASE-COHERENT LASER PULSE TRAINS

A. The NMR approach

The effects of most multiple-pulse sequences are critically dependent on the relative phases of the pulses involved. For example, assume that two pulses with flip angles $\theta = 90°$ are to be applied at the exact transition frequency ($\Delta\omega = 0$), as in Fig. 2. If the two pulses are precisely in phase the effects are additive and a complete population inversion is achieved. If they are exactly out of phase there is no net effect; the first rotation is about the x axis and the second rotation is about the $-x$ axis. Thus, if the relative phase is not specified, the final state of the system is almost completely unpredictable.

Radio frequency pulse sequences with essentially square pulses and precisely controlled phases are readily generated by the method illustrated in Fig. 3. A continuous wave at frequency ω is split into several components with different phases (usually four components in quadrature). Switches then select one of these waves.

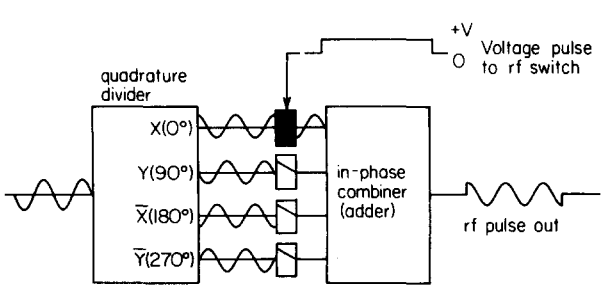

FIG. 3. Schematic of the standard pulse generation technique for NMR spectroscopy. A single rf wave is split into four components is quadrature. An rf pulse with one of these phases is produced by applying a dc pulse to the switch controlling the corresponding component. A combiner then reduces these four lines to one. In this configuration pulse lengths, pulse phases, and delays between pulses are independently controlled.

Since a switch is either on or off the amplitude is always either ω_1 or 0, neglecting pulse ringing and rise time effects. After the different pulse lines are combined, the relative phase of any two pulses is determined by noting the relative phases of the original continuous waves. Due to the advanced state of rf–microwave technology, reproducible results from sequences with thousands of pulses have been demonstrated,[16] with pulse-to-pulse fluctuations below limits of detection.

B. Pulsed laser beam splitting

The first technique used to produce laser pulse trains[29] involved splitting the output of a pulsed laser, forcing the two parts of the beam to travel along different paths, and then recombining them (Fig. 4). If, e.g., two pulses separated by 10 ns are required, then the path length difference is set to 3 m, the distance light travels in that time. Beam splitters and mirrors are the only equipment needed. The delay line can be motorized, so that the delay between pulses can be readily controlled. In addition, pulses with virtually any length or power can be handled. As a result, this approach has been widely used for photon echo experiments[29–31] and a few other simple sequences.

Unfortunately, it is very difficult to set the relative phase between two pulses with this technique, because the phase difference depends on the exact number of wavelengths in the path difference. If, collinear pulses are used, then the pulses are in phase throughout the sample if the path difference is an integral number of wavelengths. If it is half-integral, they are exactly out of phase, and so forth. Thus a 10 ns (3 m) delay line would have to be stable, measurable, and settable to ~ 10 nm to know the phase relation within ~ 5° at optical frequencies. This constraint is exceedingly difficult to meet, so that the relative phase is almost always unknown.

Under some circumstances the relative phase difference can be determined without knowing the precise delay length. If, the inhomogeneous linewidth is small enough to cause no dephasing in the time between

pulses, then the excited state population after the second pulse will give the phase relationship (see Fig. 2).[32] Multiple pulse trains have been designed to help measure pulse phases to very high precision in NMR[33] and under some circumstances these will work as well in optical spectroscopy. However, when the inhomogeneous broadening is larger than the pulse bandwidth, as is usually the case, neither of these methods will work easily. As a result, this method has generally been restricted to experiments in which the relative phase is unimportant.

C. Intracavity electro-optic modulation

A voltage pulse applied to an intracavity electro-optic modulator (EOM) changes the effective cavity length and hence the laser resonance frequency[6] (Fig. 5) and this frequency switching can be used to monitor coherent transients of the sample. In this technique, if the frequency change is much larger than the inhomogeneous linewidth, then the laser is effectively off when the voltage pulse is off. But this constraint is frequently very difficult to meet and most experiments have used frequency shifts which are much less than the inhomogeneous linewidth.[6,35] In effect, the laser is always on resonance. In addition, inspection of Fig. 5 shows that the phase difference between two pulses is equal to the frequency shift (in radians) times the delay between the pulses, so that pulse phases and delays are coupled.

The coupling between pulse phase and pulse delay frequently introduces oscillations in the observed signal, as shown in Fig. 6 for a three-pulse echo.[22] If the second pulse occurs at a time τ_1 after the first, then the phase ϕ_2 of the second pulse is $\Delta\tau_1$ ($\Delta \equiv \omega_2 - \omega_1$ is the electro-optic frequency shift and $\phi_1 = 0$ for convenience). If the third pulse occurs at a time τ_2 after the second then the phase ϕ_3 of the third pulse is $\Delta(\tau_1 + \tau_2)$. The echo intensity is proven later in this paper to be

$$I(\tau_1, \tau_2) = S(\tau_1 - \tau_2)\exp[-(\tau_1 + \tau_2)/T_2]\cos(2\phi_2 - \phi_3 - \phi_1)\,, \tag{21}$$

$$= S(\tau_1 - \tau_2)\exp[-(\tau_1 + \tau_2)/T_2]\cos\Delta(\tau_1 - \tau_2)\,, \tag{22}$$

$S(\tau_1 - \tau_2)$ is the echo shape function, which is roughly

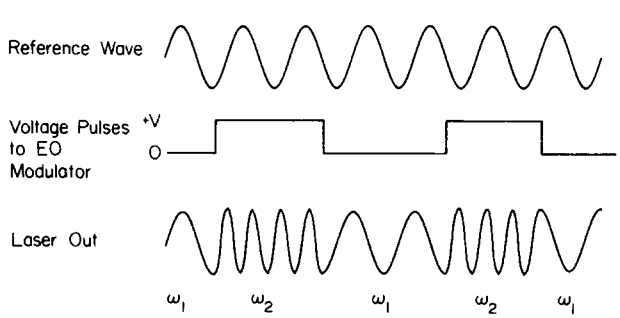

FIG. 5. Generation of laser multiple pulse trains by electro-optic modulation. An intracavity modulator changes the effective cavity length when a voltage is applied, thus shifting the laser frequency. However, $\omega_1 - \omega_2$ is generally mush less than inhomogeneous linewidths. In addition, the relative phase of two pulses separated by a time τ is $(\omega_1 - \omega_2)\tau$, so phase and delay are coupled.

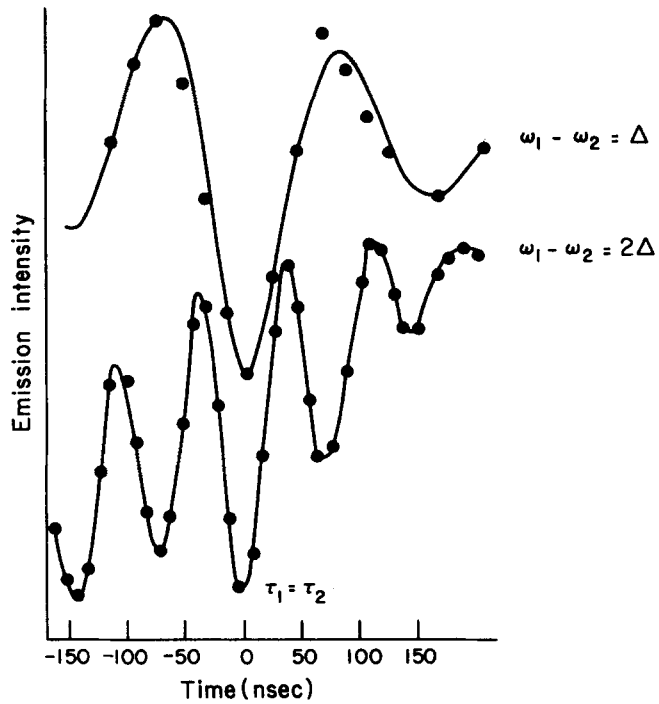

FIG. 6. Beat patterns on three-pulse echoes from electro-optic modulation. Incrementing the second delay τ_2 increments the phase of the third pulse as well, and this causes oscillations as explained in the text. These experimental data were reproduced from Ref. 22.

triangular for small flip angle pulses in highly inhomogeneous systems. The $\cos\Delta(\tau_1 - \tau_2)$ arises solely from the EOM phase shifts, as can be seen experimentally by noting that the beat frequency doubles when Δ is doubled.

An extracavity EOM can be used to compensate for these phase shifts by changing the effective path length, but the electronics would probably be quite complicated for a long pulse sequence, since the correction voltage would have to change whenever any delay is changed. In any event, multiple-pulse sequences have not been demonstrated by this method.

D. Extracavity acousto-optic modulation: Generation of multiple phase-coherent pulses

Acousto-optic laser modulation provides a simple technique[22] for producing pulse trains with known pulse lengths, delays, and phases. Furthermore, it allows one to effectively turn the laser off.

When an rf pulse train $B_1(t)$ is applied at the acoustic phonon frequency of the modulating crystal, a traveling sound wave is produced which can diffract an incident single-mode laser beam $E_{1_{in}}(t)$ into a different direction[36–38] (Fig. 7). Wave vector matching conditions imply that the diffracted laser $E_{out}(t)$ is up converted or down converted by the rf frequency, depending on the relative configuration of the laser and the modulator; only one sideband is produced if only traveling waves are applied, since only one rf wave vector and one input laser wave vector are present. Writing the rf pulse train as in Eq. (1) and assuming that the laser input $E_{1_{in}}(t)$ is perfectly monochromatic gives

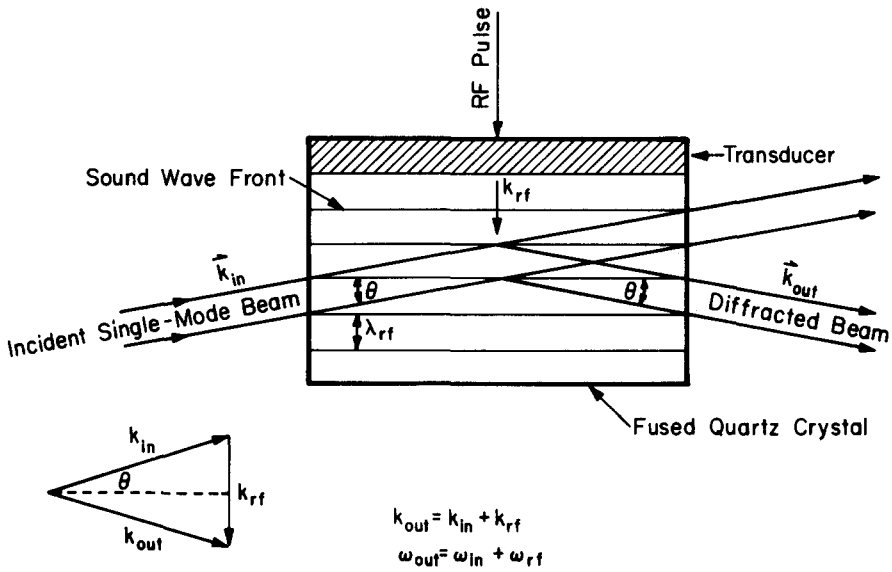

FIG. 7. An acousto-optic modulator sets up a traveling acoustic wave in response to an rf pulse. This traveling wave acts like a grating, diffracting a portion of an incident single-mode laser into a different direction. Wave vector matching conditions dictate that, for the illustrated configuration, the diffracted laser is upconverted by the rf frequency. As explained in the text, phase shifting the rf must phase shift the laser pulse out by the same amount. Taken from Ref. 38.

$$B_1(t) = \omega_1(t) \exp[i\omega_{rf} t + \phi(t)], \quad (23)$$

$$E_{in}(t) = A \exp[-i(\mathbf{k}_{in} \cdot \mathbf{r} - \omega_{in} t)], \quad (24)$$

$$E_{out}(t) = B\omega_1(t) \exp\{-i[\mathbf{k}_{out} \cdot \mathbf{r} - \omega_{out} t + \phi(t)]\}, \quad (25)$$

$$\mathbf{k}_{out} = \mathbf{k}_{in} + \mathbf{k}_{rf}, \quad (26)$$

$$\omega_{out} = \omega_{in} + \omega_{rf}. \quad (27)$$

Equation (25) shows that the amplitude modulation and phase modulation of the rf pulse train is precisely transferred to the laser output. In practice the beam $E_{in}(t)$ has a Gaussian transverse profile and the rise time of the laser pulses out is determined by the time required for the acoustic wave to cross the beam.

Phase shifting the rf input phase shifts the laser output by precisely the same amount. Physically, phase shifting the rf moves the traveling diffraction grating in the crystal, thus causing the peaks and valleys of the diffracted beam to be shifted. Thus, any laser train with arbitrary pulse phases, lengths, and delays can be generated by producing its rf analog at the acoustic phonon frequency of the modulator and a single frequency laser beam, and saving only the diffracted output.

Since the pulse phases and delays are decoupled the oscillatory behavior of EOM sequences does not appear. For example, if the pulses of a three-pulse echo experiment are generated with the same phase, then Eq. (21) becomes

$$I(\tau_1, \tau_2) = S(\tau_1 - \tau_2) \exp[-(\tau_1 + \tau_2)/T_2]. \quad (28)$$

The shape function $S(\tau_1 - \tau_2)$ can exhibit some oscillations due to extreme inhomogeneous broadening, as discussed later, but they are much less pronounced than in the EOM experiments.

The versatility of this technique is limited only by the power handling capabilities and rise time of the modulator. The crystal damage threshold for such common materials as SiO_2 and TeO_2 is quite high and in fact these crystals are used frequently as cavity dumpers in high power lasers. Modulator rise times are restricted with commercially available units to a few nanoseconds, but if necessary this limitation can be overcome in several different ways. For example, mode locking is commercially used to produce pulse trains in which all pulses are separated by 10–20 ns, with pulse widths much less than 1 ns, and with all the pulses having the same phase. Any other phase relation which is desired can be achieved by passing the pulse train through an extracavity AOM and phase shifting the rf between the laser pulses.

IV. EXPERIMENTAL SETUP

The experimental arrangement is shown in Fig. 8. A passively stabilized ring dye laser (Spectra Physics 380A) provided up to 550 mW of tunable single frequency power when pumped by 5 W all lines from an argon ion laser (Spectra Physics 164-09). The measured output frequency jitter was roughly 10 MHz in 1 s. A quite conservative assumption would be that the noise spectrum is white, in which case the frequency jitter would be 10 kHz in 1 μs; in fact low frequency components probably are dominant. Thus over the duration of a typical pulse sequence (a few microseconds at most) the laser could be considered "perfectly" monochromatic.

An AOM (Spectra Physics 481) was driven by 10 W rf pulses at 470 MHz. These pulses were produced by home built circuitry which was entirely equivalent to a conventional NMR transmitter section (shown in the dotted section of the figure). Four different phases in quadrature could be selected. With this modulator, which is several years old, rise times of 10 ns and laser diffraction efficiencies of 15%–20% were observed. More modern units are far superior; we have now produced 4 ns rise times with up to 70% diffraction efficiency.

The pulses were spatially filtered from the undiffracted beam and transmitted to the sample, which in these experiments was a gas bulb with a cold finger containing I_2. The I_2 was purified according to the proce-

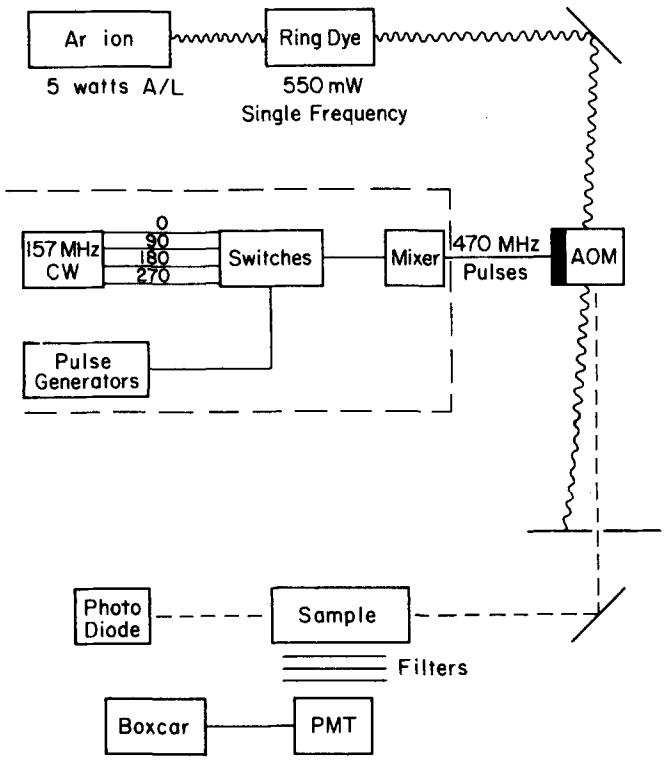

FIG. 8. Experimental configuration. The dotted section is equivalent to a conventional NMR transmitter section and produces an rf pulse train at 470 MHz. The rf pulse train produces an identical optical pulse train in the diffracted beam of the acousto-optic modulator (AOM). Spatial filtering rejects the undiffracted beam. Off-resonance fluorescence is monitored by a PMT with sharp-cut filters.

dure outlined in Ref. 22. The laser intensity (excitation frequency 5897 Å) was monitored with a photodiode. Off-resonance fluorescence from the sample was observed perpendicular to the laser using the appropriate filters and a PMT. The signal was processed by a boxcar integrator (PAR Model 162) which was configured to sweep pulse delays in the echo experiments.

V. MULTIPLE-PULSE SEQUENCES AND FLUORESCENCE DETECTION[22]

In this section we will calculate the effects of several pulse sequences, under the assumption that $\omega_1 \gg |\Delta\omega(\mathbf{q})|$, T_2^{-1}, and T_1^{-1}. Then relaxation and inhomogeneous broadening effects can be ignored during any pulse.

These assumptions can be rewritten as:

$$\gamma B_1 \gg \Delta\omega\ ,\quad T_2^{-1}\ ,\quad T_1^{-1}\ \text{(NMR)}\ , \tag{29}$$

$$|\mu|\mathcal{E} \gg \Delta\omega\ ,\quad T_2^{-1}\ ,\quad T_1^{-1}\ \text{(optical)}\ . \tag{30}$$

Equation (29) is almost always satisfied in practice; typical proton values might be $\gamma B_1 \approx 10^5$ rad, $\Delta\omega(\mathbf{r}) = 1$ rad, $T_1^{-1} \sim T_2^{-1} = 0.1$ rad. The assumptions in Eq. (30) are less defensible, as will be shown in the next section, but for large enough laser powers and strong enough transition dipole moments they can be satisfied.

Equations (29) and (30) each contain four unknown molecular parameters (the applied field is independently measurable). The two-level system is in fact completely characterized if these parameters are measured. The only major differences between NMR and optical experiments to make these measurements comes from the differences in the equilibrium density matrix [Eq. (19)] and in detection schemes. In NMR one observes transverse magnetization, which oscillates in the laboratory frame at $\omega \sim 10^9$ Hz. The voltage this oscillation produces in a coil can be mixed with two different carrier waves, 90° out of phase with one another, to measure $\langle I_x\rangle$ and $\langle I_y\rangle$ separately. In optical spectroscopy one can observe transverse polarization ($\omega \sim 10^{15}$ Hz), detected by a photodiode or photomultiplier tube. These devices discard phase information if only one laser frequency is present, so that only $(\langle R_1\rangle^2 + \langle R_2\rangle^2)$, k, and the polarization are observable.

Another approach, developed by Zewail *et al.*[22] in the optical case is to measure fluorescence, which gives $\langle 1 + R_3\rangle$ since the fluorescence intensity is simple proportional to the number of molecules in the excited state. We will show by example in the next few sections that fluorescence detection can always be used in place of polarization detection, and that this technique is in fact far more versatile because phase information is retained.

A. Pulse sequences for T_1 and T_2 measurements: Fluorescence and polarization detection

After one pulse (assumed without loss of generality to have $\phi = 0$) the density matrix is, from Eqs. (14) and (19),

$$\begin{aligned}\rho = \mathbf{1} &- \beta(\cos^2\tfrac{1}{2}\bar{\theta} + \sin^2\tfrac{1}{2}\bar{\theta}\cos 2\xi)\sigma_z \\ &- \beta(\sin\bar{\theta}\sin\xi)\quad\ \sigma_y \\ &- \beta(\sin^2\tfrac{1}{2}\bar{\theta}\sin 2\xi)\quad\ \sigma_x\ .\end{aligned} \tag{31}$$

For any particular $\Delta\omega$ and ω_1 (i.e., fixed ξ) the maximum excited state population comes from setting the pulse width such that $\theta \equiv \sqrt{\Delta\omega^2 + \omega_1^2}\,\pi = \pi$. The maximum population change from equilibrium is $\frac{1}{2}\beta(1 - \cos 2\xi)$, which falls off rapidly as $\Delta\omega/\omega_1$ increases (Fig. 9). Since $\Delta\omega/\omega_1 \sim 1$ is a rough cutoff, the Rabi frequency ω_1

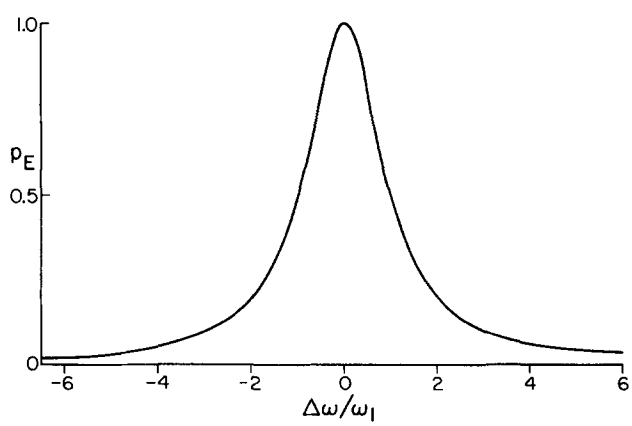

FIG. 9. Maximum possible excited state population (p_E) from one pulse as a function of resonance offset. As illustrated in Fig. 1, the pseudopolarization is generally restricted to a cone; the maximum z-axis deviation of the cone ($\bar{\theta} = 180°$) is plotted here. The maximum possible effect falls off dramatically as $|\Delta\omega/\omega_1|$ increases.

can be considered the pulse bandwidth of the laser. Monitoring fluorescence intensity I as a function of time τ after the pulse measures T_1 directly:

$$\begin{aligned} I &= \mathrm{Tr}[(1+\sigma_z)\rho(\tau)] \\ &= [\rho(\tau)]_{EE} \\ &= \sin^2 \tfrac{1}{2}\bar{\theta}(1-\cos 2\xi)\, e^{-\tau/T_1} . \end{aligned} \tag{32}$$

Since pulses generate only rotations $\langle\sigma_x\rangle^2+\langle\sigma_y\rangle^2+\langle\sigma_z\rangle^2$ is an invariant quantity, and the maximum coherence is produced by minimizing $\langle\sigma_z\rangle^2$. Minima in $\langle\sigma_z\rangle^2$ occur when

$$\begin{aligned} &\cos\bar{\theta} = -(\Delta\omega/\omega_1)^2 \quad (|\Delta\omega| < |\omega_1|) , \\ &\bar{\theta} = (2n+1)\pi \quad (|\Delta\omega| \geq |\omega_1|) . \end{aligned} \tag{33}$$

For $\Delta\omega \leq \omega_1$ the first condition gives a maximum which is always between $\bar{\theta}=\pi/2(\Delta\omega=0)$ and $\bar{\theta}=\pi(\Delta\omega=1)$; for $\Delta\omega=\omega_1$ the first condition cannot be satisfied, and $\bar{\theta}=\pi$ simultaneously maximizes excited state population and coherence. This can also be seen graphically, as in Figs. 1(a) and 1(b).

The density matrix at a time τ after the pulse has been turned off is

$$\begin{aligned} \rho(\tau) = 1 &- \beta(\cos^2\tfrac{1}{2}\bar{\theta} + \sin^2\tfrac{1}{2}\bar{\theta}\cos 2\xi)(2\,e^{-\tau/T_1}-1)\sigma_z \\ &- \beta[\cos(\Delta\omega\tau)\sin^2(\tfrac{1}{2}\bar{\theta})\sin(2\xi) \\ &+ \sin(\Delta\omega\tau)\sin\bar{\theta}\sin\xi]\, e^{-\tau/T_2}\sigma_x \\ &- \beta[\cos(\Delta\omega\tau)\sin\bar{\theta}\sin\xi - \sin(\Delta\omega\tau)\sin^2(\tfrac{1}{2}\bar{\theta})\sin(2\xi)]\, e^{-\tau/T_2}\sigma_y . \end{aligned} \tag{34}$$

If $\Delta\omega$ is perfectly uniform over the ensemble then monitoring $\langle\sigma_x\rangle$ or $\langle\sigma_y\rangle$, as in NMR, gives both $\Delta\omega$ and T_2. Monitoring $\langle\sigma_x\rangle^2+\langle\sigma_y\rangle^2$, as in the optical case, gives only a decay of $\exp(-\tau/2T_2)$ and no information on $\Delta\omega$, unless some other frequency laser is also present.[39] In that case a beat pattern will appear at frequency $\Delta\omega$.

Monitoring fluorescence after a second pulse eliminates the need for a second laser. Writing the propagator for the second pulse as U, the observed fluorescence is

$$\begin{aligned} I \sim \langle 1+\sigma_z\rangle &= \mathrm{Tr}[(1+\sigma_z)U\rho(\tau)U^+] \\ &= \mathrm{Tr}[U^+\sigma_z U\rho(\tau)] + 1 . \end{aligned} \tag{35}$$

Equation (14) shows that U^+ is derived from U by changing ρ to $-\rho$ and ξ to $-\xi$. This gives

$$I \sim A + B\,e^{-\tau/T_1} + C\,e^{-\tau/T_2} , \tag{36}$$

$$A = 1 + (\cos^2\tfrac{1}{2}\bar{\theta}_1 + \sin^2\tfrac{1}{2}\bar{\theta}_1\cos 2\xi_1)(\cos^2\tfrac{1}{2}\bar{\theta}_2 + \sin^2\tfrac{1}{2}\bar{\theta}_2\cos 2\xi_2) , \tag{37}$$

$$B = -2(\cos^2\tfrac{1}{2}\bar{\theta}_1 + \sin^2\tfrac{1}{2}\bar{\theta}_1\cos 2\xi_1)(\cos^2\tfrac{1}{2}\bar{\theta}_2 + \sin^2\tfrac{1}{2}\bar{\theta}_2\cos 2\xi_2) , \tag{38}$$

$$\begin{aligned} C = &-[\cos(\Delta\omega\tau)\sin^2(\tfrac{1}{2}\bar{\theta}_1)\sin(2\xi_1) + \sin(\Delta\omega\tau)\sin\bar{\theta}_1\sin\xi_1][\cos(\Delta\phi)\sin^2(\tfrac{1}{2}\bar{\theta}_2)\sin(2\xi_2) - \sin(\Delta\phi)\sin\bar{\theta}_2\sin\xi_2] \\ &+[\cos(\Delta\omega\tau)\sin\bar{\theta}_1\sin\xi_1 - \sin(\Delta\omega\tau)\sin^2(\tfrac{1}{2}\bar{\theta}_1)\sin(2\xi_1)][\cos(\Delta\phi)\sin\bar{\theta}_2\sin\xi_2 + \sin(\Delta\phi)\sin^2(\tfrac{1}{2}\bar{\theta}_2)\sin(2\xi_2)] , \end{aligned} \tag{39}$$

$$\Delta\phi(\mathbf{r}) = \phi_2 - \phi_1 = (\mathbf{k}_2 - \mathbf{k}_1)\cdot\mathbf{r} + (\Phi_2 - \Phi_1) . \tag{40}$$

Several points are noteworthy here. The pulses must be nearly collinear to observe any T_2 effects, since otherwise $\Delta\phi$ will vary rapidly over a small volume, $\cos(\Delta\phi)$ and $\sin(\Delta\phi)$ will average to 0, and then Eq. (39) shows that C will vanish. In addition, if $\bar{\theta}_1=\bar{\theta}_2$, $\xi_1=\xi_2$, and $\Delta\phi=\pi/2$, then $C=0$ and only T_1 decay is observed. Finally, Eqs. (38) and (39) show that, in the general case, incrementing $\Delta\phi$ by π (i.e., inverting the second pulse) has no effect on B but multiplies C by -1. This could also be seen by noting that the σ_z coefficient of $U^+\sigma_z U$ is unaffected by a 180° phase shift, but the σ_x and σ_y coefficients are inverted (Fig. 10). A sum spectrum thus gives T_1 and a difference spectrum gives T_2.

Since this last result depends only on the final pulse it is not restricted to two-pulse sequences, or for that matter to two-level systems. In general, transverse polarization can be cleanly detected (no matter what $\bar{\theta}$ or ξ is) by giving one pulse, measuring the fluorescence, and then seeing how the fluorescence changes if the pulse is phase shifted by 180°. This is the optical analog of phase sensitive detection,[21] (Fig. 11). The excited state population is detected if no pulse is applied. A linear combination of excited and ground state population is detected by taking the average fluorescence (instead of the fluorescence difference) after a 180° phase shift.

B. Echo experiments: Two and three pulses

The experiments detailed above will give all four molecular parameters (T_1, T_2, $\Delta\omega$, and $|\mu|$), if $\Delta\omega$ is uniform over the sample. If not, then the apparent T_2 from these experiments will be dominated by the inhomogeneous resonance frequency distribution. Spin echo[7] or photon echo[29] sequences are known to overcome this broadening.

For the two-pulse[29–31] and three-pulse[22] echo [Fig. 12(a)] the signal as a function of $\Delta\omega$ is most readily calculated for times τ such that $\langle(\Delta\omega-\overline{\Delta\omega})^2\rangle^{1/2}\tau \gg 1$ and $\tau \ll T_1, T_2$. Relaxation effects can then be ignored and only the average over τ corresponds to observable signal. For the three-pulse echo, e.g., the signal can be calculated as

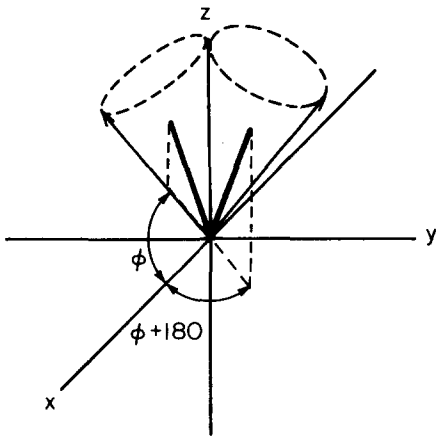

FIG. 10. Illustration of the effects on fluorescence of a 180° phase shift in the final pulse of a pulse train. The fluorescence is proportional to $(1+\sigma_z)$; if the final pulse propagator is U, this corresponds to $(1+U^*\sigma_z U)$ immediately before that pulse. The σ_x and σ_y components of this expectation value are inverted by phase shifting the pulse, which corresponds to switching between these two cones, but the 1 and σ_z components are unaffected. Thus, the sum samples only populations; the difference samples only transverse polarization.

$$\langle 1+\sigma_z\rangle = \mathrm{Tr}[(1+\sigma_z)V\Gamma_2 W\Gamma_1 U(1-\sigma_z)U^*\Gamma_1^\dagger W^*\Gamma_2^\dagger V^*]$$
$$= 1-\mathrm{Tr}(\sigma_z V\Gamma_2 W\Gamma_1 U\sigma_z U^*\Gamma_1^\dagger W^*\Gamma_2^\dagger V^*)$$
$$= 1-\mathrm{Tr}(V^*\sigma_z V)(\Gamma_2 W\Gamma_1)(U\sigma_z U^*)(\Gamma_1^\dagger W^*\Gamma_2^\dagger)\ , \qquad (41)$$

where U, W, and V are the three-pulse propagators, and $\Gamma_i = \exp(-i\mathcal{H}\tau_i)$ is the evolution between pulses. Saving only terms which are time independent when $\tau_1 = \tau_2$, and defining $A = U\sigma_z U^*$ and $B = V^*\sigma_z V$, gives

$$\langle 1+\sigma_z\rangle = 1-2A_{11}B_{11}(|W_{11}|^2-|W_{12}|^2)$$
$$-2\,\mathrm{Re}[A_{12}B_{12}(W_{12}^*)^2]\exp[-i\Delta\omega(\tau_1-\tau_2)]\ . \qquad (42)$$

Phase shifting the third pulse by 180° multiplies B_{12} by -1, so the difference spectrum (which detects only transverse polarization, as mentioned earlier) gives:

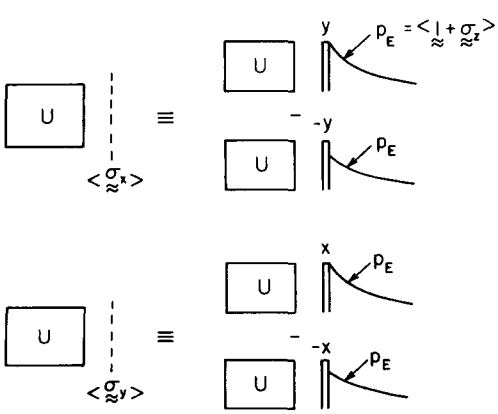

FIG. 11. Optical phase sensitive detection can be generally achieved by including one more pulse in the multiple pulse train, monitoring fluorescence, and observing the change in fluorescence if the pulse is phase shifted by 180°.

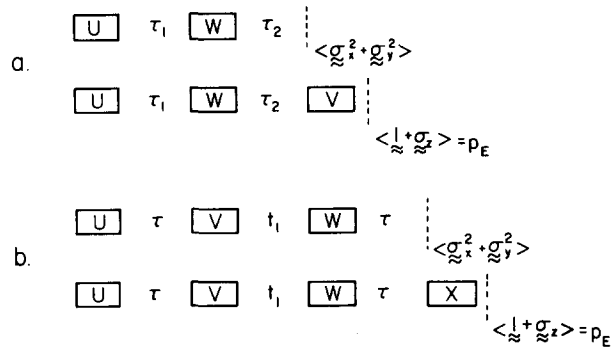

FIG. 12. Echo pulse sequences. The sequences in part (a) are photon echoes to refocus inhomogeneous braodening, with the two versions differing only in the detected operator. The sequences in part (b) are called stimulated echoes and are discussed in the text of this paper and our following paper on mutlilevel systems.

Three-pulse echo

$$= -2\,\mathrm{Re}\{A_{12}B_{12}(W_{12}^*)^2\exp[-i\Delta\omega(\tau_1-\tau_2)]\} \qquad (43)$$
$$= -2\,\mathrm{Re}\{V_{11}U_{11}^*U_{12}V_{12}W_{21}^2\exp[-i\Delta\omega(\tau_1-\tau_2)]\}\ . \qquad (44)$$

Similar calculations for the two-pulse echo give:

$$\text{Two-pulse echo} = |U_{11}^*U_{12}W_{21}^2\exp[-i\Delta\omega(\tau_1-\tau_2)]|^2\ . \qquad (45)$$

The two-pulse echo has the following properties:

(1) It is totally independent of the relative phase of the pulses, since only magnitudes appear in Eq. (45). However, it does correspond to a direction $\mathbf{k}_3 = 2\mathbf{k}_2 - \mathbf{k}_1$,[40] as can be seen by explicitly writing out the dependence of U_{12} on $\mathbf{k}_1$ and W_{21} on $\mathbf{k}_2$ as in Eq. (40).

(2) W_{21} is maximized when $\bar{\theta}_2 = \pi$ no matter what ξ_2 or ϕ_2 is, as can be seen in Eq. (14). But $|U_{11}^*U_{12}|$ is the transverse polarization produced by the first pulse, which is maximized under the constraints given with Eq. (33). Thus, the "90-τ-180-τ" echo sequence only maximizes the signal near resonance, and for $\Delta\omega \gtrsim \omega_1$ two equal pulses are in fact superior.

(3) The echo decays as $e^{-\tau/T_2}$. This is not apparent from a density matrix transformation such as this one, but falls out immediately when relaxation effects are included as in a superoperator approach.

The three-pulse echo has somewhat different properties:

(1) The pulse phases are quite important. If $\theta_1 = \theta_2$ and $\xi_1 = \xi_2$ [which will always be a constraint for maximizing the signal, from the equal roles they plan in Eq. (44)] then we can write (when $\tau_1 = \tau_2$)

three-pulse echo

$$= -|U_{11}^*|\,|U_{12}^2|\,|W_{21}^2|\cos(2\phi_2-\phi_1-\phi_3)\ . \qquad (46)$$

If the three pulses are not collinear the echo will vanish. If they are collinear, three equal phases will give a maximum negative echo [i.e., a dip in the baseline generated by the first two terms of Eq. (42)]. Phase shifting the first or third pulse by 180°, or by the second pulse by 90°, turns this dip exactly into a peak, as illus-

trated in Fig. 13.

Another way to view this effect of phase shifting is to note that detection of $\langle 1+\sigma_x\rangle$ after the final pulse corresponds to detection of $\langle 1+\alpha\sigma_x+\beta\sigma_y+\gamma\sigma_z\rangle$ immediately before that pulse, where α, β, and γ depend on the pulse flip angle, pulse phase, and resonance offset. Here $\langle 1+\gamma\sigma_z\rangle$ corresponds to populations which decay by spontaneous emission or other T_1-type mechanisms; $\langle\alpha\sigma_x+\beta\sigma_y\rangle$ corresponds to the desired phase sensitive detection, but this coefficient is frequently much smaller than the population term, so that a small echo is observed on a large spontaneous emission base line (Fig. 14). The echo at $\tau=\tau'$ will decay as $e^{-2\tau/T_2}$ as the delays are changed, but the sloping base line makes quantitative measurements difficult.

Phase shifting the last pulse by 180° is equivalent to introducing an additional 180° rotation about the z axis. This changes the detected operator from $\langle 1+\alpha\sigma_x+\beta\sigma_y+\gamma\sigma_z\rangle$ to $\langle 1-\alpha\sigma_x-\beta\sigma_y+\gamma\sigma_z\rangle$. The echo is exactly inverted, but the spontaneous emission background is unchanged, so a difference spectrum (final pulse of some specific phase minus final pulse shifted by 180°) removes the background (Fig. 14). The slightly oscillatory behavior of the echo is discussed later.

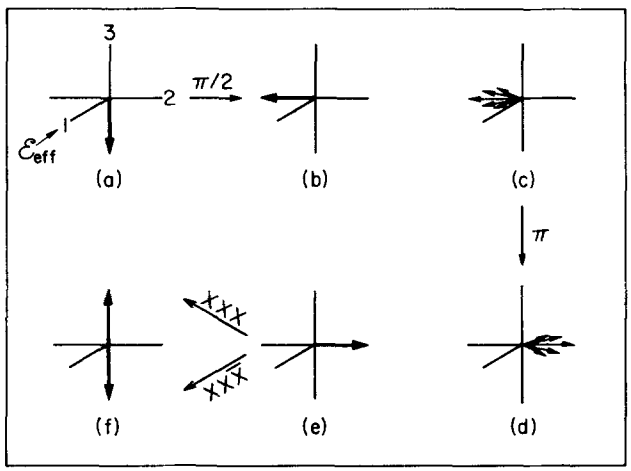

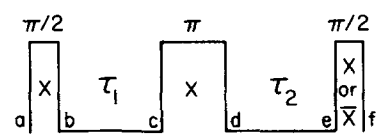

FIG. 13. Gyroscopic model of the three-pulse echo with fluorescence detection. The phase of each pulse is written in the standard NMR notation (x: $\phi=0$, y: $\phi=\pi/2$, $\bar{x}$: $\phi=\pi$, $\bar{y}=3\pi/2$). After the first pulse (assumed here to have a pulse bandwidth much larger than the resonance offset) transverse polarization disappears rapidly because of the inhomogeneous resonance frequency distribution. The second pulse refocuses this broadening, just as in a NMR spin echo. The final state produced by the third pulse depends on that pulse's phase, see also Fig. 2. The fluorescence is proportional to the echo height (transverse polarization prior to the last pulse), but it has a large spontaneous emission base line. A difference spectrum ($\times\times\times - \times\times\bar{x}$) then suppresses the base line.

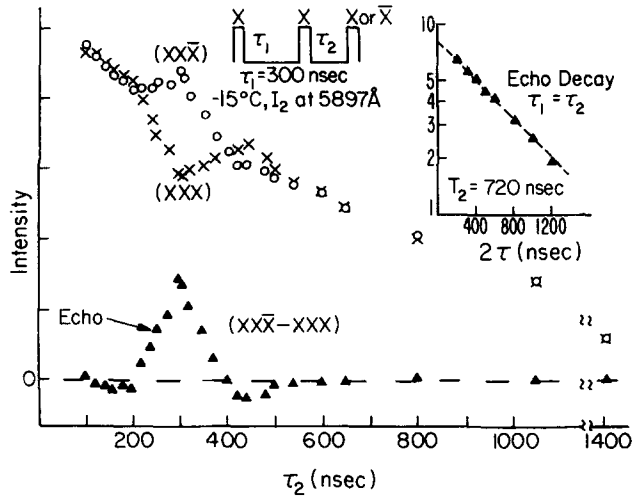

FIG. 14. Experimental three-pulse echo line shape for I_2 gas at −15°C. Phase shifting the third pulse turns the small dip into a peak; the difference spectrum has no spontaneous emission background and a clean exponential decay for $\tau_1=\tau_2$ giving T_2. The echo line shape is oscillatory, as can be seen here and in Fig. 19.

(2) W_{21}^2 is maximized by $\bar{\theta}_2=\pi$, as before. The terms in U and V are maximized by the constraints in Eq. (33). Thus, near resonance the maximum signal is given by (90-τ-180-τ-90); far from resonance three equal pulses are better.

(3) The echo decays as $e^{-2\tau/T_2}$.

C. Stimulated echo sequences: Three and four pulses

The first pulse sequence in Fig. 12(b) is called a stimulated echo sequence. In an ensemble of closed noninteracting two-level systems such as we are discussing it has quite simple properties. These properties are most easily illustrated for the four pulse version (which has not been previously reported) because of its inherent symmetry:

$$\langle\sigma_x\rangle=-\mathrm{Tr}(\sigma_x X\Gamma W T V\Gamma U\sigma_x U^{\dagger}\Gamma^{\dagger}V^{\dagger}T^{\dagger}W^{\dagger}\Gamma^{\dagger}X^{\dagger})$$

$$=\sum_{ij}(V\Gamma U\sigma_x U^{\dagger}\Gamma^{\dagger}V^{\dagger})_{ij}$$

$$\times(W^{\dagger}\Gamma^{\dagger}X^{\dagger}\sigma_x X\Gamma W)_{ij}\exp[-i(\omega_i-\omega_j)t_1]\,, \qquad (47)$$

where $T=\exp(-i\mathcal{H}t_1)$ and $\Gamma=\exp(-i\mathcal{H}\tau)$. The first operator in parenthesis is the density matrix after the second pulse. The second operator is the time reversed version of the first. The terms with $i=j$ (populations) decay with time constant T_1; the terms with $i\neq j$ decay with time constant T_2^*, the inhomogeneous lifetime. We will discuss these sequences further in the following paper, in the context of multilevel systems.

VI. REAL TWO-LEVEL SYSTEMS: EXTREME BROADENING AND POPULATION DEPLETION

The effects of all the pulse sequences discussed in the last section change dramatically as the resonance offset is increased. The simple vector pictures which show, e.g., that two-pulse echoes are maximized by $(\pi/2)$

$-\tau-\pi$ near resonance must be substantially modified, and the signal maximization constraints are quite different. However, the assumption was made in the last section that the inhomogeneous broadening is much less than the pulse bandwidth, and under those conditions the off-resonance effects are basically a curiosity, since then $\Delta\omega \sim 0$ can be achieved simultaneously for all parts of the ensemble.

In real optical systems the assumptions of Eq. (30) rarely hold. Inhomogeneous broadening mechanisms such as Doppler widths, crystal strains, and natural abundance of isotopic species typically produce linewidths of 0.01–1 cm^{-1}, corresponding to $\langle\Delta\omega^2\rangle^{1/2} \sim 2$–200 G rad/s. Only a laser which gives 90° pulses ($\omega_1 t_p = \pi/2$) in less than 1 ns can turn over the entire profile on the low end of this inhomogeneous range, and on the high end pulse widths of ~10 ps are needed. Even then, the power requirements are fairly stringent. If $\mu = 0.05$ D and the laser beam diameter is 1 mm (which are the conditions encountered in the gas phase experiments detailed here) then a peak laser power of 10^7 W is needed for a 10 ps pulse to be a $\pi/2$ pulse. The beam can be focused more tightly in crystals, but not in gas phase experiments because of the transverse velocity distribution. The power requirement goes down by a factor of 4 when the pulse width is doubled, but most picosecond laser systems have fixed pulse widths.

As a result, almost all optical experiments in fact use pulse bandwidths which are at best comparable to the inhomogeneous broadening, and often the bandwidths are orders of magnitude less than the broadening. Under these conditions the off-resonance effects are no longer a curiosity but are a central feature of any experiment.

The population relaxation rate T_1, e.g., is no longer uniquely defined, and different experiments can measure different values. The traditional NMR approach is to give a sequence π-τ-$\pi/2$ and measure the transverse magnetization as a function of τ; this magnetization will decay as $(2e^{-\tau/T_1} - 1)$. This sequence has also been used in optical domain experiments,[34] where the inhomogeneous broadening guarantees that the decay will also have a T_2 dependence. If an EOM is used to generate frequency shifted laser pulses then the T_2 terms oscillate and can be removed, as shown earlier. However, the T_1 measured is not simply the time which a molecule spends in the excited state. It is instead the time which a molecule spends in the portion of the excited state which is within the pulse bandwidth. Velocity-changing collisions would take the molecule off resonance, so that such collisions would look like a T_1 mechanism, and the measured T_1 would depend on the laser bandwidth. On the other hand, such collisions have no effect on the fluorescence lifetime, so the T_1 from this type of measurement can be different.

A. Open systems and relaxation: An example for pulse sequence design in gases

Another assumption which often does not hold but which affects T_1 measurements is that the two-level system can be considered closed. Even if the energy level structure is sparse, so that the laser is only near resonance for transitions from some particular ground state G to a particular excited state E, many relation mechanisms force a complete analysis to include other states. For example, the most important relaxation mechanism at optical frequencies is often spontaneous emission. Normally transitions from E to many other ground states G' will also be allowed, so that on the average E does not relax simply to G (Fig. 15). Collisions can cause population transfers between G and G', between E and other excited states E', or between E and G' (collisional deactivation).

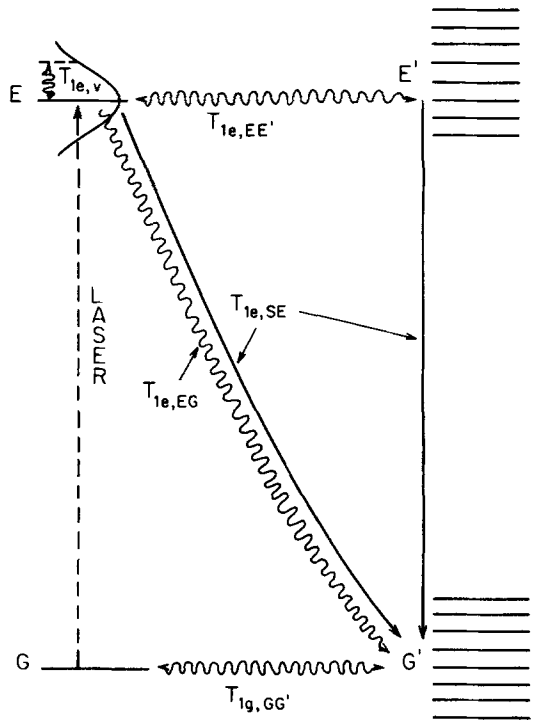

FIG. 15. Schematic energy level diagram for real optical transitions in gases. The exciting laser transfers population from G to E, which decays radiatively to other ground states G' ($T_{1e,SE}$) or nonradiatively to states E' or G'. Collisions can also take any individual molecule out of the laser bandwidth (T_{1ev}) or can establish thermal equilibrium ($T_{1g,GG'}$).

Strictly speaking, these relaxation mechanisms involve many levels, and the transitions should be explicitly treated as part of a multilevel system. We will assume here, however, that coherences involving E' or G' can be neglected, and treat these as "bath states." The time dependence of the populations can be written from inspection of Fig. 15 as:

$$\dot{p}_E(t) = -p_E(t)/T_{1e,SE} - p_E(t)/T_{1e,v} - p_E(t)/T_{1e,E'} - p_E(t)/T_{1e,G'} , \tag{48}$$

$$\sum \dot{p}_{E'}(t) = -\sum p_{E'}(t)/T_{1e,SE} - \sum p_{E'}(t)/T_{1e,EG'} + p_E(t)/T_{1e,EE'} , \tag{49}$$

$$\dot{p}_G(t) = +[1 - p_G(t)]/T_{1g,GG'} , \tag{50}$$

$$\sum \dot{p}_{G'}(t) \sim 0 . \tag{51}$$

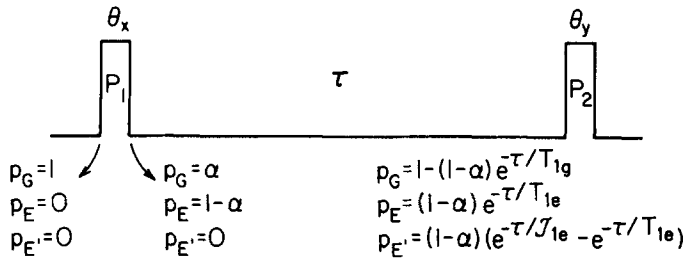

FIG. 16. Simply pulse sequence to measure T_{1e} and T_{1g}. The two pulses are phase shifted by 90° to destroy any T_2 effects [see Eq. (39)]. The fluorescence decay as a function of τ, minus the decay which would be observed by omitting pulse p_2, is biexponential with two equally intense components. The pulse shape and flip angles reflect only α, which appears simply as a scale factor.

After P_2 : $\langle p_E + p_{E'} \rangle = (1-\alpha)(1-(1-\alpha)e^{-\tau/T_{1g}}) + \alpha(1-\alpha)e^{-\tau/T_{1e}} + (1-\alpha)(e^{-\tau/\mathcal{T}_{1e}} - e^{-\tau/T_{1e}})$

Without P_2: $\langle p_E + p_{E'} \rangle = (1-\alpha)e^{-\tau/\mathcal{T}_{1e}}$

Difference : $\langle p_E + p_{E'} \rangle = (1-\alpha) - (1-\alpha)^2 e^{-\tau/T_{1g}} - (1-\alpha)^2 e^{-\tau/T_{1e}}$

These equations assume that there are many states G' and E', that no individual E' is ever substantially populated, that most of the equilibrium population is in states G', and that all the states E' have equal collisional and spontaneous emission rates to G. Under these assumptions Eqs. (48)–(51) can be solved to give

$$p_E(t) = p_E(0)\, e^{-t/T_{1e}}, \tag{52}$$

$$\sum p_{E'}(t) = p_E(0)(e^{-t/\mathcal{T}_{1e}} - e^{-t/T_{1e}}), \tag{53}$$

$$p_G(t) = 1 - [1 - p_G(0)]\, e^{-t/T_{1g}}, \tag{54}$$

$$T_{1e}^{-1} = T_{1e,SE}^{-1} + T_{1e,EG'}^{-1} + T_{1e,EE'}^{-1} + T_{1e,v}^{-1}, \tag{55}$$

$$\mathcal{T}_{1e}^{-1} = T_{1e,SE}^{-1} + T_{1e,EG'}^{-1}, \tag{56}$$

$$T_{1g}^{-1} = T_{1g,GG'}^{-1}. \tag{57}$$

There are thus at least three distinct relaxation times, and under less stringent assumptions even more parameters would be needed. All of these can be extracted from simple pulse sequences. Fluorescence decays measure $p_E(t) + \sum p_{E'}(t)$, which decays as a simple exponential with time constant $\mathcal{T}_{1e}$. The pulse sequence (π)-τ-$(\pi/2)$ with detection of induced polarization would give a biexponential decay with distinct T_{1e} and T_{1g} components if off-resonance effects could be neglected. However the first pulse produces substantial polarization when $\Delta\omega \neq 0$, as shown in Fig. 1. This means that the observed decay will have a superimposed signal which depends on the exact pulse lengths and even on the pulse shapes, since the exact amount of polarization produced for any given value of $\Delta\omega$ is sensitive to both of these factors. In highly inhomogeneous systems this additional signal is substantial, and the observed decay cannot be readily interpreted.

T_{1e} and T_{1g} can also be measured by detecting the fluorescence after P_x-τ-P_y, where the two pulses are identical except for the 90° phase shift. The shift ensures that the decay has no T_2 dependence, as was mentioned earlier [Eq. (36)]. This decay is triexponential with time constants $\mathcal{T}_{1e}$ (from the population in states E' off resonance with the laser at time τ immediately before the second pulse), T_{1e} (from the population in state E), and T_{1g} (from the population in state G). The $\mathcal{T}_{1e}$ dependence can be removed by subtracting the one-pulse fluorescence intensity at time $\tau + \tau_p$, where τ_p is the pulse width, because the difference spectrum samples only the states which are affected by the second pulse (Fig. 16). The difference is biexponential with equal amounts of T_{1g} and T_{1e} decay. Since biexponentials are notoriously difficult to fit experimentally this simplification of the decay is quite useful.

We have used this technique to measure low pressure lifetimes in I_2. At -30 and -50 °C the two-pulse decay appears as a simple exponential and had the same lifetime as the fluorescence, indicating $T_{1e} \sim \mathcal{T}_{1e}$ and either $T_{1g} \sim T_{1e}$ or $T_{1g} \gg T_{1e}$. At -12 °C (Fig. 17) the difference spectrum displayed a clearly different decay rate for short times than did the fluorescence ($T_{1e} = 400 \pm 100$ ns, $\mathcal{T}_{1e} = 850 \pm 50$ ns). If collisional cross sections for the ground and excited states are equal, then $T_{1e}^{-1} = \mathcal{T}_{1e}^{-1} + T_{1g}^{-1}$ which predicts $T_{1g} \sim 800$ ns. In fact we observe $T_{1g} = 2200 \pm 200$ ns, implying a smaller collisional cross section for the ground state. Further measurements will be reported later,[41] but it is clear that the results of previous measurements, which have been mainly interpreted from a two-level perspective, must be examined.

B. Optimizing pulse sequences

Exteme inhomogeneous broadening also implies that the observable signal from any multiple pulse experiment must be integrated over $\Delta\omega$, which leads to quite different results than were discussed earlier. Consider the effects of applying one pulse and monitoring fluorescence. What pulse length maximizes the signal? For any $\Delta\omega$, the maximum was shown earlier to be $\bar{\theta} = \theta[1 + (\Delta\omega/\omega_1)^2]^{1/2} = \pi$. If this constraint is satisfied for one particular value of $\Delta\omega$, it is clearly not satisfied everywhere else. For example, $\theta = \omega_1 t_p = \pi$ gives the maximum signal on resonance, but this signal falls off steeply as $\Delta\omega/\omega_1$ increases as shown in Fig. 18(a), because for all other values of $\Delta\omega$ the pulse is too long.

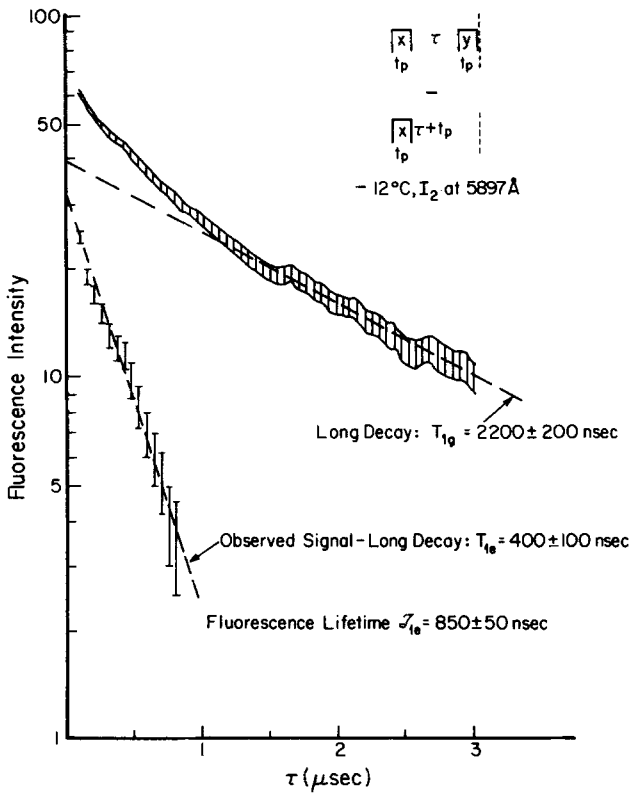

FIG. 17. Measurement of ground state (T_{1g}) and excited state (T_{1e}) relaxation rates at −12° in I_2. The fluorescence decay for the sequence $\theta_x - \tau - \theta_y$, minus the fluorescence present if the last pulse is eliminated, should be biexponential with roughly equal coefficients for the two rates, as seen here. The implied collisional cross section is small for the ground state (see the text).

Smaller pulse flip angles are superior. Integration over all values of $\Delta\omega$ can be done by computer and such calculations show the maximum signal corresponds to $\theta \sim 138°$ [Fig. 18(b)].

Another form of inhomogeneous broadening which must usually be considered is laser inhomogeneity. If the laser is operating in TEM_{00} mode then the transverse intensity profile is Gaussian. A pinhole can be used to "cut out" the wings; however the tightly focused lasers required for high power density expand substantially over short distances from the beam waist, so the combination of high homogeneity and high power density is difficult to achieve. In addition, cutting out the beam wings is counterproductive, because much of the observed fluorescence is generated there. Since the laser intensity falls off in the wings, the optimum pulse flip angle is expected to increase when a Gaussian transverse profile is assumed. This is in fact what happens, and the new maximum is found (again by using a computer to average in the contribution from the wings) to be at $\theta \sim 200°$.

Similar unusual effects can be seen with other pulse sequences. Since equal pulses were shown [Eqs. (43)–(45)] to give the largest two-pulse or three-pulse echo intensity far from resonance, it is not surprising that averaging over the entire profile gives optimum pulse

TABLE I. Flip angles for real optical two-level systems.

Maximum excited state population:	
No inhomogeneity	180° pulse
Inhomogeneous transition homogeneous laser	138° pulse
Inhomogeneous transition Inhomogeneous laser	~200° pulse
Maximum echo:	
No inhomogeneity	90–τ–180–τ–90
Inhomogeneous transition Homogeneous laser	80–τ–160–τ–80 (100–τ–110–τ–110 3% less)
Inhomogeneous transition Inhomogeneous laser	100–τ–220–τ–110 (170–τ–170–τ–170 1% less)

ratios which differ from the standard 1:2 or 1:2:1. The maximum two-pulse echo (ignoring laser inhomogeneity) is computed to occur at a ratio of about 1:1.7. The effects on three-pulse echoes are more dramatic; three equal pulses perform almost as well as a 1:2:1 ratio (see Table I). This result is useful experimentally, because trains of equal pulses are often simpler to implement.

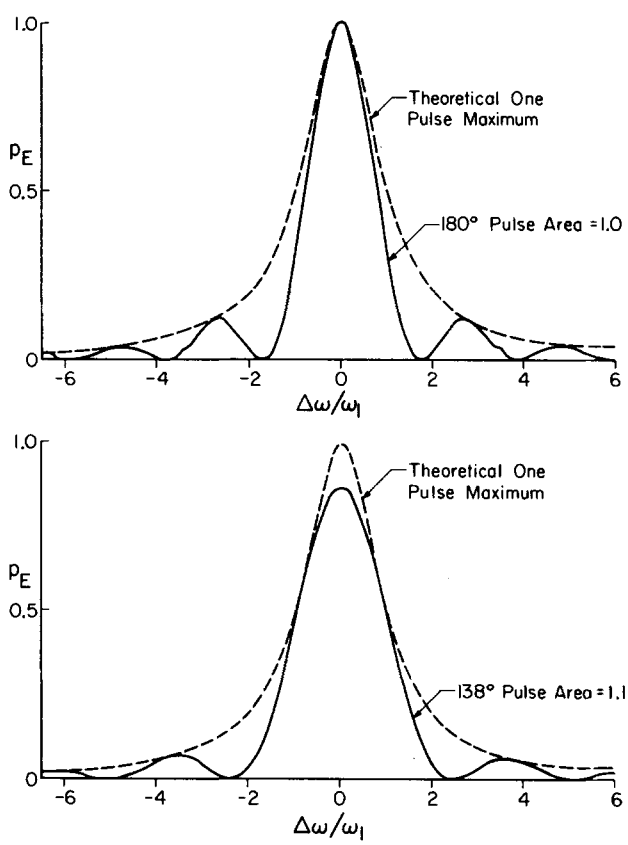

FIG. 18. The population inversion from one pulse on resonance as a function of $\Delta\omega$, compared to the theoretical maximum of Fig. 9. A pulse with $\bar{\theta} = 180°$ creates a complete inversion on resonance, but the effects die out rapidly as $\Delta\omega$ increases. $\bar{\theta} = 138°$ is not as good on resonance, but its effects fall off more slowly, making the total excited state population (and hence total fluorescence) larger.

The three-pulse echo has a slightly oscillatory behavior similar to that previously predicted in optical spectroscopy[42] and observed in NMR[43] for large flip angle free induction decays and two-pulse echoes. In all these cases the oscillations are produced because the coherence magnitude or echo intensity does not decline smoothly to zero as the resonance offset increases. In three-pulse echo experiments oscillations occur even for fairly small flip angles, as shown in the Appendix. Most of our experiments involved three equal pulses, after verifying that in highly inhomogeneous systems this configuration works almost exactly as well as a 1 : 2 : 1 ratio. Under these conditions computer simulations of our experiment show dips both after and before the echo peak, as seen in Figs. 14 and 19. The echo line shape is essentially a smoothed triangular function for small flip angles. The echo width increases as pulse flip angles increase; the echo height reaches a maximum and then declines. The 100 ns pulses at the top of Fig. 19 correspond to roughly 60° at the peak of the laser's Gaussian intensity profile, as verified by line shape simulations.

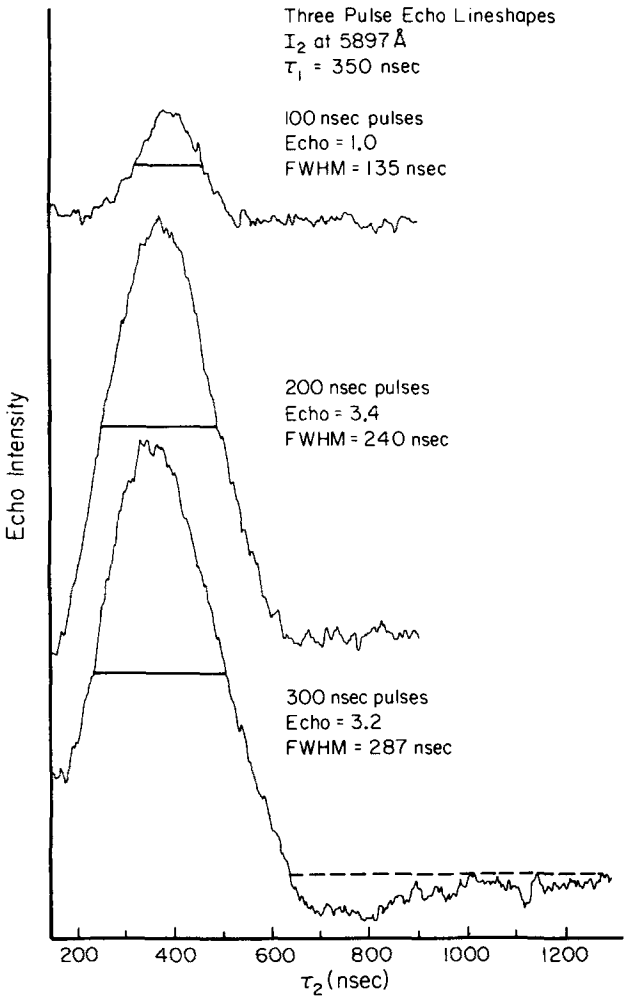

FIG. 19. Three-pulse echo difference line shapes (×××−××R) as a function of pulse flip angle. For small flip angles the line shape is essentially a smoothed triangular function (exact expressions are given in Appendix). Echo width increases as the pulse flip angle is increased, but echo height (the number in parentheses) reaches a maximum and then declines. For large flip angles the echo is oscillatory. The 100 ns pulses correspond to roughly 60° at the peak of the transverse laser profile, as verified by line shape simulations.

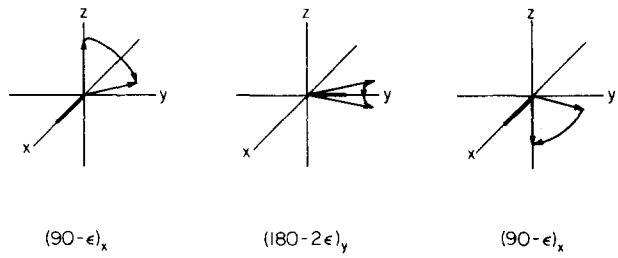

FIG. 20. Illustration of the response of the composite 180° pulse $(90_x-180_y-90_x)$ to an inhomogeneous rf or laser field. If the first pulse is 90° at the peak intensity, it will be somewhat less than 90° at other points. Still, to lowest order in the deviation ϵ, no residual transverse component is produced (the first correction term is proportional to ϵ^2). A simple $(180°-2\epsilon)$ pulse would leave a transverse component of 2ϵ. Thus, this sequence is inherently compensated for field inhomogeneities. It is also compensated for transition inhomogeneity, as discussed in the text. This compensation is the fundamental reason for the widespread interest in composite pulse trains in NMR.

C. Composite pulse trains

It has been known for many years in NMR that several pulses back-to-back can be less sensitive to inhomogeneities than is a single pulse.[44] For example, rf inhomogeneities make it impossible for any single pulse to be a π pulse throughout a real sample. A $\pi/2$ pulse, followed immediately by a π pulse 90° out-of-phase, followed immediately by a $\pi/2$ pulse of the original phase [written in the NMR convention as $(\pi/2)_x-(\pi)_y-(\pi/2)_x$, where the subscripts reflect the rotation axis in the xy plane] improves on this substantially, since it cancels the rf inhomogeneity to lowest order[44] (Fig. 20). There have also been some applications of composite pulse trains to compensate for transition inhomogeneity; this same pulse sequence creates large population inversions even for $\Delta\omega/\omega_1 \sim 1$, where the effects of a single pulse have substantially diminished.

The case $\Delta\omega \gg \omega_1$ is of little interest in NMR, but as we have shown is quite important in optical spectroscopy. Composite laser pulses are capable of turning over a larger fraction of the inhomogeneous profile far from resonance, thus effectively increasing the laser bandwidth and increasing the observable signal. Consider, e.g., the case $\Delta\omega=\omega_1$. The maximum excited state population from a single pulse is produced by $\bar{\theta}=\pi$ (Fig. 21). After this pulse the excited state and ground state populations are equal. Increasing $\bar{\theta}$ decreases the excited state population because the polarization vector is constrained to stay along a fixed cone. Phase shifting the radiation by 180° changes the cone, so another pulse with $\bar{\theta}=\pi$ creates a complete population inversion.

The excited state population produced by several different sequences as a function of $\Delta\omega$ was calculated using Eqs. (14) and (19) and is shown in Figs. 22 and 23.

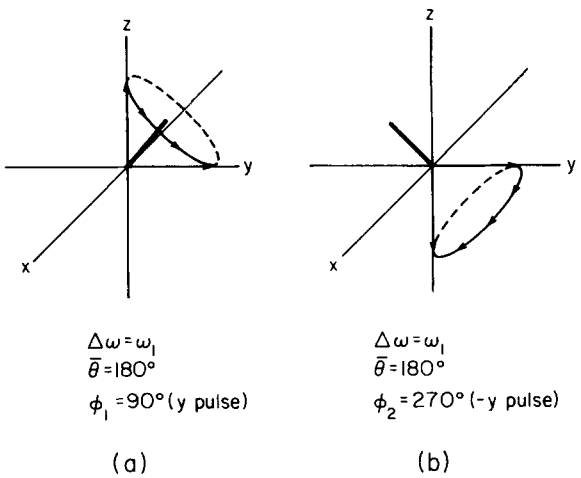

FIG. 21. As shown in Fig. 2, a single pulse can only create a complete population inversion for $\Delta\omega = 0$. Composite pulses can achieve this for other values of $\Delta\omega$. For example, if $\Delta\omega = \omega_1$ a single pulse can take σ_z down to σ_y, but no further; a second pulse, phase shifted by 180° from the first, changes the rotation axis and takes σ_y to $-\sigma_z$. Thus complete inversions are possible far from resonance.

In a highly broadened system the area under these curves is the only observable quantity. This area is somewhat increased by two pulses (Fig. 22) and substantially increased by two different "composite π pulses" (Fig. 23). The sequence $90_x - 180_y - 90_x$ is very good near resonance; the sequence $60_x - 300_{-x} - 60_x$ has large spikes far from resonance but has a greater overall area, as shown in Fig. 23.

The transverse Gaussian profile of laser intensity must also be included to compare these results with experiment. Table I shows that the largest number of molecules in the excited state (and hence the largest fluorescence intensity) is produced by a 200° pulse. Composite pulses increase this intensity as demonstrated experimentally in Fig. 24, with an 82% improvement observed for $(60_x - 300_{\bar{x}} - 60_x)$. Our composite pulse experiments were compared to theoretical predictions in Table II by neglecting pulse rise times but assuming that the pulses were separated by 20 ns gaps, which corresponded to what we observed with a fast photodiode; the numbers in that table come from integrating over curves similar to those presented in Figs. 22 and 23. The agreement, which is generally excellent, serves as a sensitive test of pulse phase, and confirms that the rf phases were transferred cleanly to the optical pulses.

We also verified that three-pulse echoes can be enhanced by composite pulses, as shown in Fig. 25. This figure compares the difference spectrum from three equal 300 ns pulses (the spectrum for all three pulses

TABLE II. Fluorescence intensity after one composite pulse.[a]

Pulse	Experimental	Theoretical
200_x	1	1
$100_x - 100_y$	1.08	1.14
$100_x - 100_{\bar{x}}$	1.16	1.19
$60_x - 300_x - 60_x$	1.03	1.04
$60_x - 300_{\bar{x}} - 60_x$	1.82	1.87

[a]Observed and predicted fluorescence intensities after a single composite pulse. The theoretical prediction is based on square pulses with 20 ns gaps, assuming a Gaussian distribution to the laser intensity.

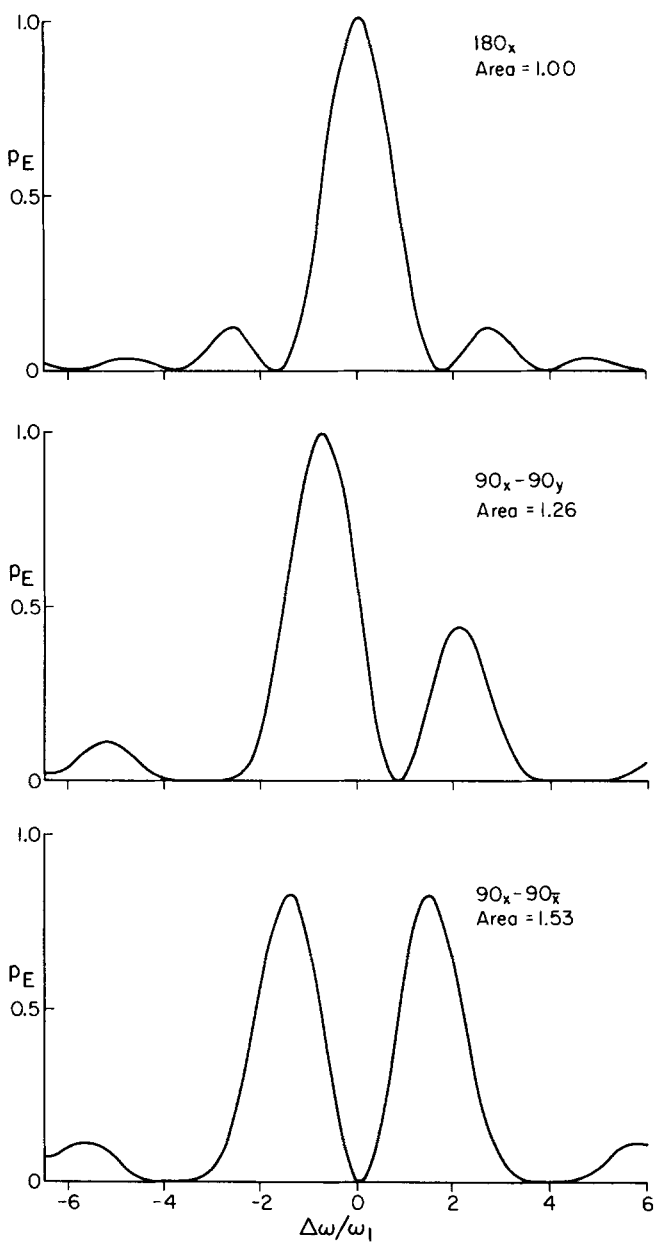

FIG. 22. Excited state populations produced by two-pulse composites as a function of $\Delta\omega$, compared to the effects of a single pulse. Fluorescence signals from a highly inhomogeneous transition will be proportional to the area under these curves, which is larger for the composite pulse trains. Thus the signal is enhanced, yet these sequences are no longer than a single 180° pulse.

in phase is similar to Fig. 14) with the spectrum obtained by replacing each 300 ns pulse by 150 ns of one phase, followed in less than 10 ns by a 150 ns pulse of opposite phase. The composite pulse echo is taller and narrower, as would be expected if the effective bandwidth was increased.

Both the simple and composite pulse echoes show some oscillatory behavior, but the oscillations are much more pronounced in the composite case. These oscillations can be predicted by calculating the expected echo intensity as a function of $\Delta\omega$ (Fig. 26). The intensity pattern has strong structural features. Fourier transforming to get the dependence on τ_2 gives good agreement with experiment. More structured composite pulses are expected to produce even larger oscillations.

Even better sequences than these certainly exist, but there is usually a trade-off between improving the bandwidth versus keeping the total duration of the pulse train

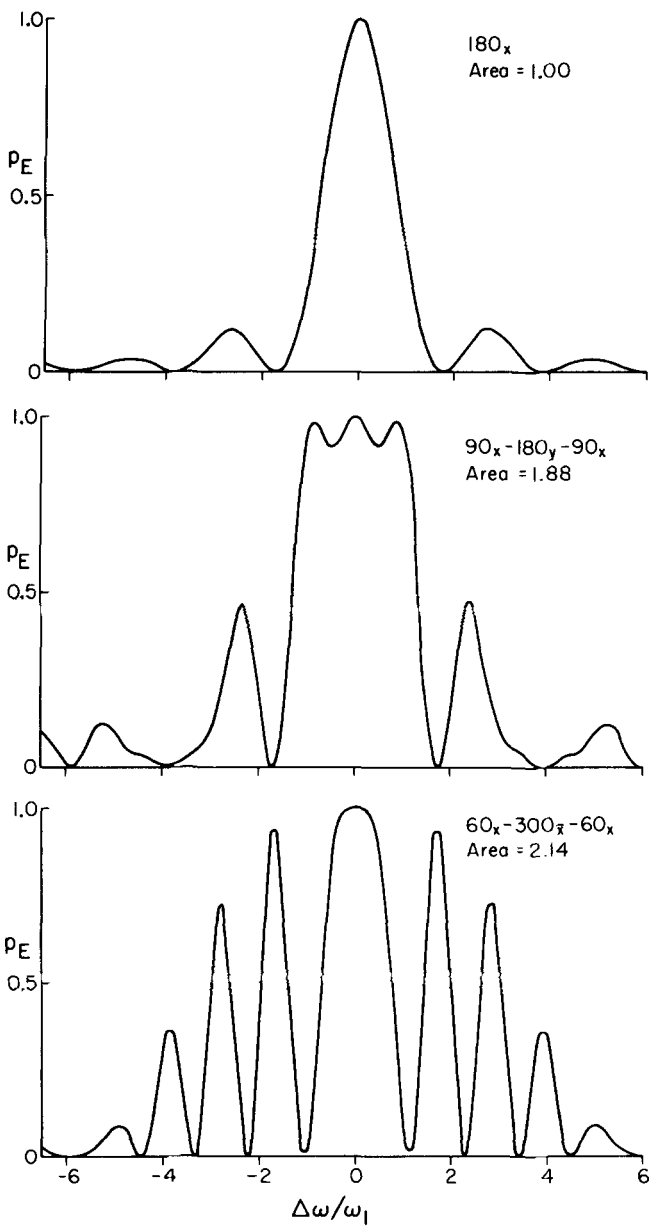

FIG. 23. The effects of more complex composite pulse sequences. The sequence $(90_x - 180_y - 90_x)$ is a good 180° pulse over a wide range of values of $\Delta\omega$, as is well known in NMR, and thus is very useful for slightly broadened transitions. Highly broadened transitions give larger signals for the sequence $60_x - 300_{-x} - 60_x$.

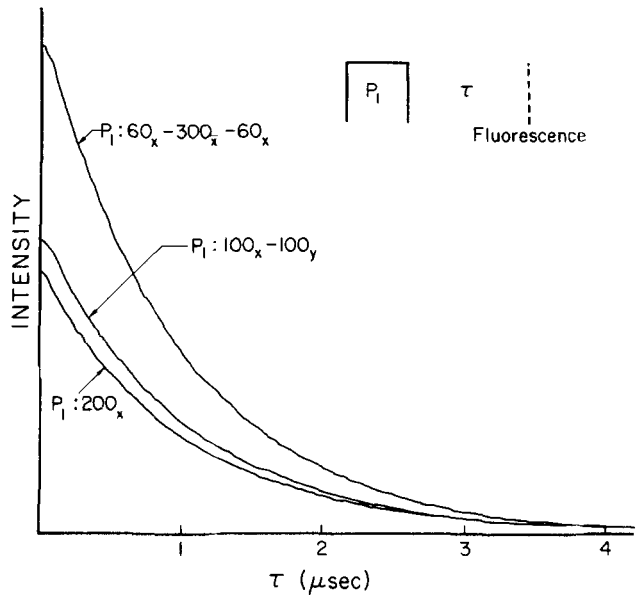

FIG. 24. Fluorescence decays after composite pulse trains. The maximum single pulse fluorescence occurs after a 200° pulse. Composite pulse trains are more effective in exciting transitions far from resonance, as explained in the text, therefore the fluorescence increases.

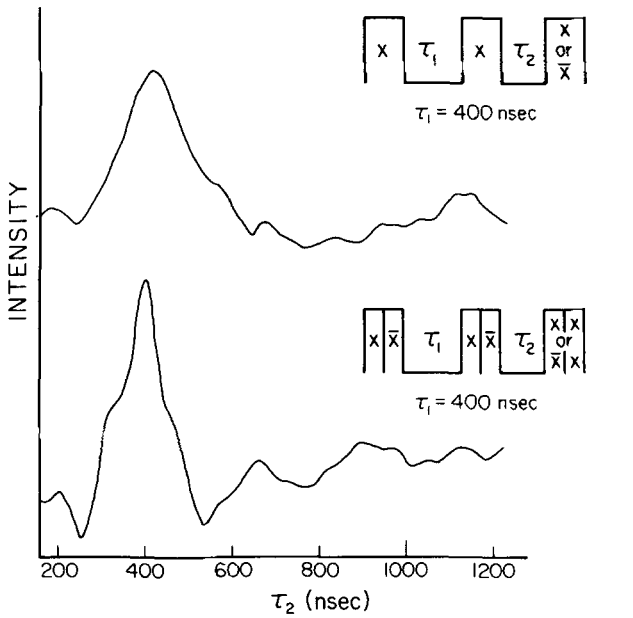

FIG. 25. Composite pulse trains can also enhance three-pulse photon echoes. The top echo line shape was generated by taking $\times\times\times - \times\times\bar{\times}$ for 300 ns pulses, thus suppressing the background as in Figs. 14 and 19. The bottom spectrum was generated by replacing each 300 ns pulse with 150 ns of one phase, immediately followed by 150 ns exactly out of phase. The echo is taller and sharper, reflecting the larger effective pulse bandwidth. The composite pulse echo is also more oscillatory.

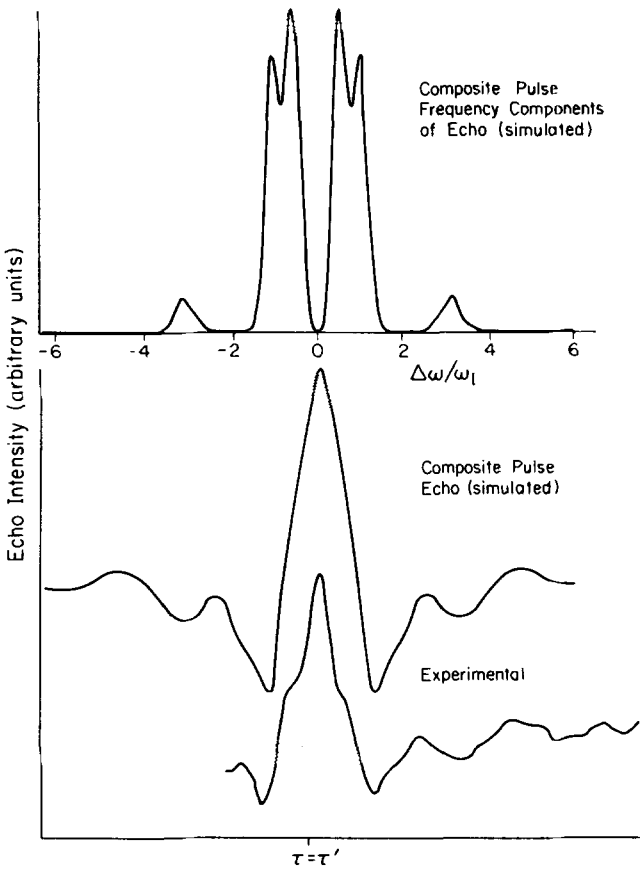

FIG. 26. The composite pulse echo oscillations are expected because the echo intensity as a function of resonance offset $\Delta\omega$ is highly structured, as seen in the computer simulation at the top. Fourier transformation gives the expected echo line shape, which agrees well with experiment.

short. Designing an optimum pulse train is largely an exercise in computer programming, although systematic criteria for optimizing composite pulse trains can sometimes be derived.[45,46]

VII. CONCLUSIONS

In this paper we have used the techniques of AOM and fluorescence detection, developed by Zewail *et al.*[22], to demonstrate that phase-coherent laser multiple pulse trains are technically possible, and that they can be used for a number of new applications: (i) generation of phase sensitive (quadrature) detection: (ii) suppression of spontaneous emission backgrounds from three-pulse echo experiments; (iii) measurements of additional relaxation parameters in systems with complex rotational-vibrational levels; and (iv) enhancement of effective laser bandwidths through composite pulse trains.

We will report on further applications in the next paper, in the context of multilevel systems. In a third coming paper we discuss selective multiquantum excitation.[46]

ACKNOWLEDGMENTS

W. R. Lambert's generous help in the initial stage of this work is greatly appreciated; his expertise and efforts facilitated our success in observing these transients. We also wish to thank Russell Chipman and Ed Sleva for experimental assistance. This work was supported by the National Science Foundation under Grant No. DMR81-05034.

APPENDIX: CALCULATION OF ECHO LINE SHAPES

We start with Eq. (44):

$$I(\tau_1,\tau_2) = -2\,\mathrm{Re}\{V_{11}U_{11}^{*}U_{12}V_{12}W_{21}^{2}\exp[-i\Delta\omega(\tau_1-\tau_2)]\}\,, \quad \text{(A1)}$$

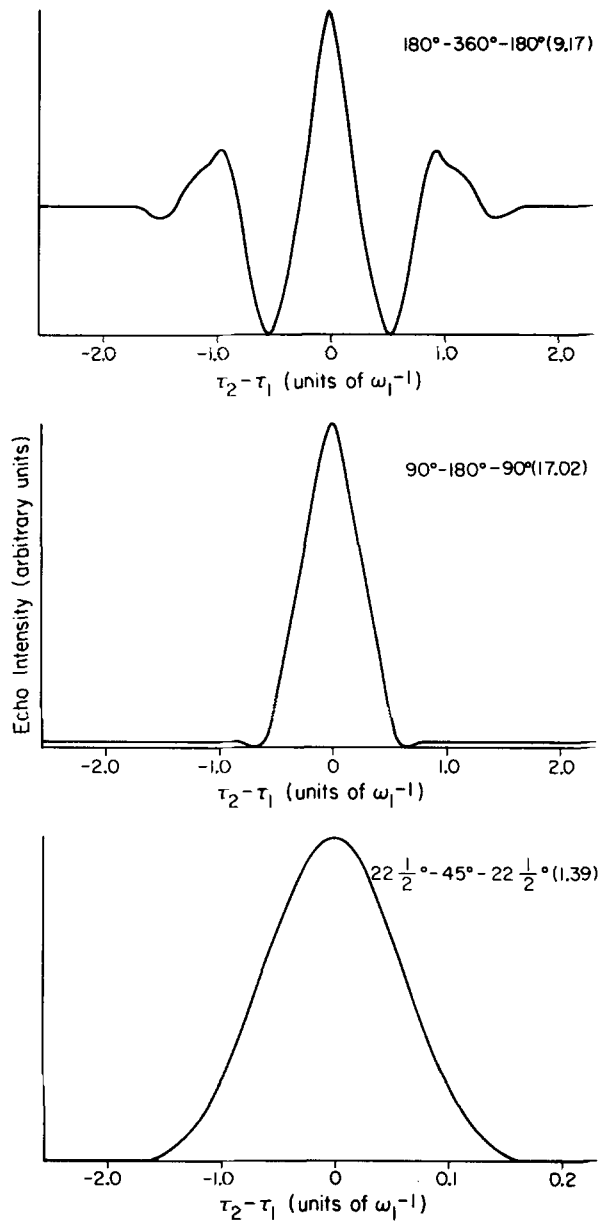

FIG. 27. Three-pulse echo line shapes for a 1:2:1 pulse ratio, with the relative full scale intensity in parentheses. Laser inhomogeneities have been neglected to better illustrate the flip angle dependence. The echoes get narrower as the flip angle increases (note the change of scale in the lowest figure). For small flip angles the line shape is closer to a smoothed triangular function than a Gaussian or a Lorentzian. For large flip angles oscillations appear. The maximum signal actually corresponds to 80–160–80, with a full scale height of 17.85.

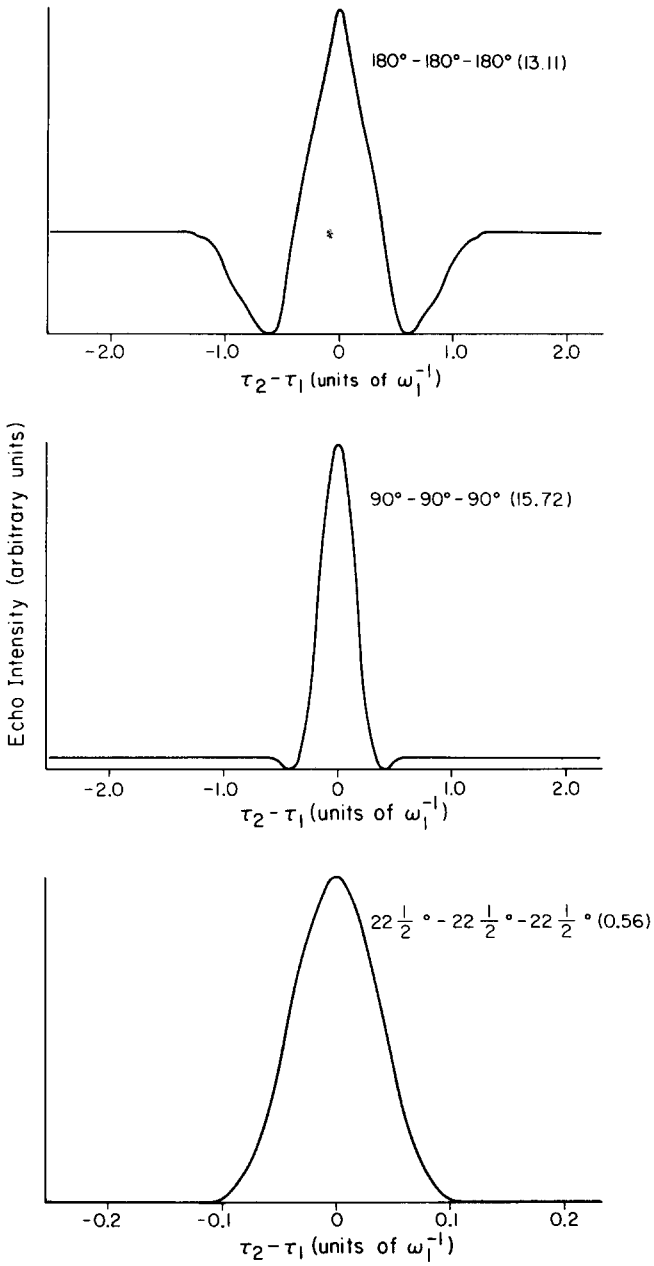

FIG. 28. Three-pulse echo line shapes for equal pulses. The maximum intensity occurs at 110-110-110, and is almost 98% of the maximum 1 : 2 : 1 echo. This effect is due to the assumption of extreme inhomogeneous broadening.

where **U**, **W**, and **V**, the propagators for the first, second, and third pulses, respectively, were given in Eq. (14). If the first and third pulses are identical (except for a possible phase shift) then $U_{11} = V_{11}$, and if the phase of the ith pulse is ϕ_i this becomes

$$I(\tau_1, \tau_2) = -2 |U_{11}|^2 |U_{12}|^2 |W_{21}|^2 \times \mathrm{Re}\{\exp[i(2\phi_2 - \phi_3 - \phi_1)] \exp[-i\Delta\omega(\tau_1 - \tau_2)]\} . \quad \text{(A2)}$$

For a highly inhomogeneously broadened transition integration over $\Delta\omega$ is required:

$$I(\tau_1, \tau_2) = \mathrm{Re}\{S(\tau_1 - \tau_2) \exp[i(2\phi_2 - \phi_3 - \phi_1)]\} , \quad \text{(A3)}$$

$$S(\tau_1 - \tau_2) = -2 \int_{-\infty}^{\infty} |U_{11}|^2 |U_{12}|^2 |W_{12}|^2 \times \exp[-i\Delta\omega(\tau_1 - \tau_2)]\, d(\Delta\omega) . \quad \text{(A4)}$$

The shape function $S(\tau_1 - \tau_2)$ is the Fourier transform (F.T.) of the transform of the intensity at the peak of the echo ($\tau_1 = \tau_2$) as a function of $\Delta\omega$. Unfortunately, S is generally quite complicated. In the case of three pulses with a 1 : 2 : 1 length ratio and a first pulse flip angle $\theta = \omega_1 t_p$, Eq. (A4) can be rewritten using Eq. (14) as

$$S(\tau_1 - \tau_2) \sim \text{F.T.} \left[\sin^4 \tfrac{1}{2}\bar{\theta} \cos^2 \tfrac{1}{2}\bar{\theta} \left(\frac{\omega_1 t_p}{\bar{\theta}}\right)^4 - \sin^6 \tfrac{1}{2}\bar{\theta} \left(\frac{\omega_1 t_p}{\bar{\theta}}\right)^6\right] , \quad \text{(A5)}$$

$$\bar{\theta} = \Delta\omega \sqrt{1 + (\omega_1^2/\Delta\omega^2)} . \quad \text{(A6)}$$

Computer evaluation of $S(\tau_1 - \tau_2)$ shows that it corresponds to a smooth, monotonically decreasing function of $|\tau_1 - \tau_2|$ for small flip angles, with small oscillations appearing as the flip angles increase. If all three pulses have equal lengths then the expression for $S(\tau_1 - \tau)$ is

$$S(\tau_1 - \tau_2) \sim \text{F.T.} \left[\sin^4 \tfrac{1}{2}\bar{\theta} \left(\frac{\omega_1 t_p}{\bar{\theta}}\right)^4 - \sin^6 \tfrac{1}{2}\bar{\theta} \left(\frac{\omega_1 t_p}{\bar{\theta}}\right)^6\right] , \quad \text{(A7)}$$

which becomes oscillatory for smaller values of θ than does Eq. (A5), as shown in Figs. 27 and 28. Experimental verification for these oscillations is given in Figs. 14 and 19.

[1] F. Bloch, Phys. Rev. 70, 460 (1946).
[2] F. Bloch, W. W. Hansen, and M. Packard, Phys. Rev. 70, 474 (1946).
[3] E. M. Purcell, H. C. Torrey, and R. Pound, Phys. Rev. 69, 37 (1946).
[4] A. Abragam, *The Principles of Nuclear Magnetism* (Oxford, University, London, 1963).
[5] T. C. Farrar and E. D. Becker, *Pulse and Fourier Transform* NMR (Academic, New York, 1971).
[6] For a recent review see: M. Burns, W. Liu, and A. H. Zewail, *Modern Problems in Solid State Physics* (North-Holland, Amsterdam, 1982), Vol. 20.
[7] E. L. Hahn, Phys. Rev. 77, 297 (1950).
[8] H. Y. Carr and E. M. Purcell, Phys. Rev. 94, 630 (1954).
[9] S. Meiboom and G. Gill, Rev. Sci. Instrum. 29, 688 (1958).
[10] U. Haeberlen and J. S. Waugh, Phys. Rev. 175, 453 (1968); J. S. Waugh, L. M. Huber, and U. Haeberlen, Phys. Rev. Lett. 20, 180 (1968); P. Mansfield, J. Phys. C 4, 1444 (1971); W.-K. Rhim, D. D. Elleman, and R. W. Vaughan, J. Chem. Phys. 58, 1772 (1973).
[11] U. Haeberlen, *Advances in Magnetic Resonance* (Academic, New York, 1976), Suppl. 1.
[12] D. P. Burum and W.-K. Rhim, J. Chem. Phys. 71, 944 (1979).
[13] M. E. Stoll, A. J. Vega, and R. W. Vaughan, J. Chem. Phys. 67, 2029 (1977).
[14] S. Vega, T. W. Shattuck, and A. Pines, Phys. Rev. Lett. 37, 43 (1976); G. Drobny, A. Pines, S. Sinton, D. P. Weitekamp, and D. Wemmer, Faraday Symp. Chem. Soc. 13, 49 (1979).
[15] G. Bodenhausen, R. L. Vold, and R. R. Vold, J. Magn. Reson. 37, 93 (1980); A. Wokaun and R. R. Ernst, Chem. Phys. Lett. 52, 407 (1977); H. Hatanaka, T. Terao, and T. Hashi, J. Phys. Soc. Jpn. 39, 835 (1975).

[16]W. S. Warren, S. Sinton, D. P. Weitekamp, and A. Pines, Phys. Rev. Lett. 43, 1791 (1979); W. S. Warren, D. P. Weitekamp, and A. Pines, J. Chem. Phys. 73, 2084 (1980); W. S. Warren and A. Pines, *ibid.* 74, 2808 (1981).
[17]A. G. Redfield, Sara V. Kunz, and E. K. Ralph, J. Magn. Reson. 19, 114 (1975).
[18]W. P. Aue, E. Bartholdi, and R. R. Ernst, J. Chem. Phys. 64, 2229 (1976).
[19]R. H. Dicke, Phys. Rev. 93, 99 (1954).
[20]R. P. Feynman, F. L. Vernon, and R. W. Hellwarth, J. Appl. Phys. 28, 49 (1957).
[21]W. S. Warren and A. H. Zewail, J. Chem. Phys. 75, 5956 (1981).
[22]A. H. Zewail, T. E. Orlowski, K. E. Jones, and D. E. Godar, Chem. Phys. Lett. 48, 256 (1977); T. E. Orlowski, K. E. Jones, and A. H. Zewail, Chem. Phys. Lett. 54, 197 (1978); T. E. Orlowski and A. H. Zewail, J. Chem. Phys. 70, 1390 (1979); A. H. Zewail, Acc. Chem. Res. 13, 360 (1980) and references therein.
[23]J. A. Armstrong and E. Courtens, IEEE J. Quantum Electron. QE-4, 411 (1968); QE-5, 249 (1969).
[24]I. I. Rabi, N. F. Ramsey, and J. Schwinger, Rev. Mod. Phys. 26, 157 (1964).
[25]R. Loudon, *The Quantum Theory of Light* (Oxford, London, 1973), Chap. 7; A. Yariv, *Quantum Electronics* (Wiley, New York, 1975).
[26]A. Redfield, Adv. Magn. Reson. 1, 1 (1966).
[27]G. Binsch, in *Dynamic Nuclear Magnetic Resonance Spectroscopy*, edited by L. M. Jackson and F. A. Cotton, (Academic, New York, 1975).
[28]R. A. Hoffman, Adv. Magn. Reson. 4, 88 (1970).
[29]N. A. Kurnit, I. D. Abella, and S. R. Hartmann, Phys. Rev. Lett. 13, 567 (1964); I. D. Abella, N. A. Kurnit, and S. R. Hartmann, Phys. Rev. 141, 391 (1966).
[30]D. E. Cooper, R. W. Olson, R. D. Wieting, and M. D. Fayer, Chem. Phys. Lett. 67, 41 (1979).
[31]W. H. Hessilink, and D. A. Wiersma, Chem. Phys. Lett. 56, 227 (1978); M. de Vries, P. de Bree, and D. A. Wiersma, *ibid.* 52, 399 (1977).
[32]H. P. Grieneisen, J. Goldhar, N. A. Kurnit, J. Javan, and H. R. Schlossberg, Appl. Phys. Lett. 21, 559 (1972).
[33]U. Haubenreiser and B. Schnabel, J. Magn. Reson. 35, 175 (1979).
[34]R. G. Brewer and R. L. Shoemaker, Phys. Rev. A 6, 2001 (1972).
[35]Typical switching frequencies are about 50 MHz, which is much less than the inhomogeneous broadening.
[36]R. Alder, IEEE Spectrum 4, 42 (1967); R. Z. Bachrach, Rev. Sci. Instrum. 43, 734 (1972).
[37]J. Sapriel, *Acousto-Optics* (Wiley, New York, 1978).
[38]T. E. Orlowski, K. E. Jones, and A. H. Zewail, Chem. Phys. Lett. 54, 197 (1978).
[39]R. G. Brewer and R. L. Shoemaker, Phys. Rev. Lett. 27, 631 (1971).
[40]This point is discussed in Ref. 29.
[41]W. S. Warren, E. Sleva, and A. H. Zewail (to be published).
[42]A. Schenzle, N. C. Wong, and R. G. Brewer, Phys. Rev. A 21, 887 (1980), R. G. Brewer and A. Genack, Phys. Rev. Lett. 36, 959 (1976).
[43]M. Kunitomo, T. Endo, S. Nakanishi, and T. Hashi, Phys. Rev. A 25, 2235 (1982).
[44]R. Freeman, S. P. Kempsell, and M. H. Levitt, J. Magn. Reson. 38, 453 (1980); M. H. Levitt and R. Freeman, *ibid.* 43, 502 (1981); M. H. Levitt, R. Freeman, and T. Frenkel, *ibid.* 47, 328 (1982).
[45]J. S. Waugh, J. Magn. Reson. (in press).
[46]W. S. Warren and A.H. Zewail, J. Chem. Phys. (Flygare issue).